

The $u'g'r'i'z'$ Standard Star System

J. Allyn Smith^{1,2,3,4}, Douglas L. Tucker^{1,5}, Stephen Kent⁵, Michael W. Richmond⁶, Masataka Fukugita^{7,8}, Takashi Ichikawa⁹, Shin-ichi Ichikawa¹⁰, Anders M. Jorgensen¹¹, Alan Uomoto¹², James E. Gunn¹³, Masaru Hamabe¹⁴, Masaru Watanabe¹⁵, Alin Tolea¹², Arne Henden¹⁶, James Annis⁵, Jeffrey R. Pier¹⁶, Timothy A. McKay³, Jon Brinkmann¹⁷, Bing Chen¹², Jon Holtzman¹⁸, Kazuhiro Shimasaku¹⁹, Donald G. York^{20,21}

ABSTRACT

We present the 158 standard stars that define the $u'g'r'i'z'$ photometric system. These stars form the basis for the photometric calibration of the Sloan Digital Sky

¹Equal first authors.

²Visiting Astronomer, United States Naval Observatory.

³University of Michigan, Department of Physics, 500 East University, Ann Arbor, MI 48109

⁴Current Address: University of Wyoming, Department of Physics & Astronomy, P.O. Box 3905, Laramie, WY 82071

⁵Fermi National Accelerator Laboratory, P.O. Box 500, Batavia, IL 60510

⁶Physics Department, Rochester Institute of Technology, 85 Lomb Memorial Drive, Rochester, NY 14623-5603

⁷Institute for Cosmic Ray Research, University of Tokyo, Midori, Tanashi, Tokyo 188-8502, Japan

⁸Institute for Advanced Study, Olden Lane, Princeton, NJ 08540

⁹Astronomical Institute, Tohoku University, Aoba, Sendai 980-8578, Japan

¹⁰National Astronomical Observatory of Japan, Mitaka, Tokyo, 181-8588 Japan

¹¹Los Alamos National Laboratory, NIS-4, D448, Los Alamos, NM 87545

¹²Department of Physics and Astronomy, The Johns Hopkins University, 3701 San Martin Drive, Baltimore, MD 21218, USA

¹³Princeton University Observatory, Princeton, NJ 08544

¹⁴Department of Mathematical and Physical Sciences, Japan Women's University, Mejirodai, Tokyo, 112-8681 Japan

¹⁵Institute of Space and Astronautical Science, Sagamihara, Kanagawa 229-8510, Japan

¹⁶U.S. Naval Observatory, Flagstaff Station, P.O. Box 1149, Flagstaff, AZ 86002-1149

¹⁷Apache Point Observatory, P.O. Box 59, Sunspot, NM 88349-0059

¹⁸New Mexico State University, Dept. 4500, Box 30001, Las Cruces, NM 88003

¹⁹Department of Astronomy and Research Center for the Early Universe, School of Science, University of Tokyo, Bunkyo-ku, Tokyo, 113-0033 Japan

²⁰The University of Chicago, Department of Astronomy and Astrophysics, 5640 S. Ellis Ave., Chicago, IL 60637

²¹The University of Chicago, Enrico Fermi Institute, 5640 S. Ellis Ave., Chicago, IL 60637

Survey (SDSS). The defining instrument system and filters, the observing process, the reduction techniques, and the software used to create the stellar network are all described. We briefly discuss the history of the star selection process, the derivation of a set of transformation equations for the $UBVR_cI_c$ system, and plans for future work.

Subject headings: catalogs — stars: fundamental parameters — standards

1. Introduction

We present the newly established standard star network for the $u'g'r'i'z'$ filter system (see Fukugita et al. 1996). This standard star network was developed at the U.S. Naval Observatory, Flagstaff Station. These stars form the basis for the photometric calibration of the Sloan Digital Sky Survey (SDSS). The SDSS uses a 2.5-m telescope at Apache Point Observatory (APO) to produce a five-band, photometrically calibrated digital imaging survey of π steradians (10,000 square degrees) of the Northern Galactic Cap (Gunn et al. 1998; York et al. 2000) as one of its major data products.

It is not our purpose here to describe in detail the full end-to-end process of calibrating the SDSS photometric data. That is the topic of a future paper. Here, we merely wish to present a self-contained description of the standard star network upon which the SDSS photometry is based. We do note, however, that one of the targets of the SDSS is to achieve a level of photometric uniformity and accuracy such that the system-wide rms errors in the final SDSS photometric catalog will be less than 0.02 mag in r' , 0.02 mag in $(r' - i')$ and $(g' - r')$, and 0.03 mag in $(u' - g')$ and $(i' - z')$, for objects bluer than an M0 dwarf. To meet this target, internal goals were set for the accuracy of the primary standard star system: the uncertainty in the mean calibrated magnitudes for any given primary standard star should be $\leq 1.5\%$ at u' , $\leq 1\%$ in g', r' and i' , and $\leq 1.5\%$ at z' . As we will show later in this paper, we more than meet these goals for all but a handful of stars.

In addition, we must mention that, due to small-but-significant differences between the USNO and 2.5-m filters, the final 2.5-m SDSS published photometry will likely differ systematically from the $u'g'r'i'z'$ system at the few percent level for $g'r'i'$ and slightly worse for u' and z' (see Stoughton et al. 2001). When transformation equations between the $u'g'r'i'z'$ system and the 2.5-m SDSS photometry have been robustly determined, they will be promptly made available to the astronomical community. (Note: the intended accuracy of these transformation equations is included within the above-mentioned error budget for the photometric calibrations of the final SDSS imaging catalog.)

The nomenclature used in this system differs slightly from the traditional photometric literature. This was done to avoid confusion with existing SDSS papers and nomenclature. In the traditional sense, Vega (α Lyr) is the ultimate “fundamental” standard. However, in this paper we refer to three subdwarf stars which were used to set the initial system zeropoint as “fundamental” with the other 155 stars of the system being referred to as “primary” stars. The term “secondary” is used within the SDSS nomenclature to refer to the photometric system transfer patches — pieces

of the sky that are observed by a 0.5-m telescope that are used to transfer the photometric solution to the main survey imaging telescope.

In the following sections we present details of the standard star development program. We describe the instrumentation and filter system in §2, selection of the initial set of stars in §3, and a brief overview of the reduction software that was used to develop the network in §4. Final results for the initial set of $u'g'r'i'z'$ primary standard stars are presented in §5, and we discuss future extensions to this system in §6.

2. Observations and Instrumentation

The observations were obtained using the 1.0-m Ritchey–Chrétien telescope at the U.S. Naval Observatory’s Flagstaff Station (USNO-FS) during the bright period of each lunation from March 1998 through January 2000 inclusive. Since the program stars were fairly bright the moon did not unduly hamper the observations; however, we did maintain a minimum 30° radius of avoidance near the moon that, for the most part, allowed us to use the dome to shield the telescope from direct moonlight. This observing restriction had a slight impact on the choice of stars observed each night. The few “faint” stars (fainter than about $r'=13.2$) on the list were observed when the moon was below or within one hour of the opposite horizon from the star so the dome could be used to block the moon completely.

All of the observations were direct exposures with a thinned, UV-AR coated, Tektronix TK1024 CCD operating at a gain of 7.43 ± 0.41 electrons per ADU with a readnoise of 6.0 electrons. This CCD is similar to the CCDs used in the main SDSS survey camera and the CCD used by the 0.5-m photometric monitoring telescope at APO. The camera scale of 0.68 arcsec/pixel produced a field of view of 11.54 arcmin.

Testing of the chip revealed a linear response up to 15,200 ADU and a second, well behaved and correctable linear response region up to 27,500 ADU (see Figure 1). This change in the CCD response function, and sense of the change, is due to the clocking scheme that was employed in the TK1024 read electronics. The integration and the lowering of the transfer gate occurred simultaneously. The net result is that, since the summing well has more charge for brighter objects, the charge begins to ‘spill over’ the gate potential faster for these objects, resulting in an effective longer integration time (and a seemingly higher gain) than for the faint objects.

Exposure lengths were tailored to maximize the number of potential standard stars in each field with good photon counts in all five filters while not exceeding the first linear portion of the response curve for the primary star of interest. Tailoring the exposure lengths allowed us to develop multiple standards in several fields. Use of the linearity response curve allowed correction of the brighter stars when good atmospheric seeing caused counts greater than 15,200 ADU per pixel while allowing us to maximize observing efficiency in some of the more populated fields. The drawback of targeting multiple stars per field was a decrease in the signal to noise ratio for the extreme red

or blue stars within the same field for which the exposures were not optimized.

The five filters of the $u'g'r'i'z'$ system have effective wavelengths of 3540 Å, 4750 Å, 6222 Å, 7632 Å, and 9049 Å, respectively, at 1.2 airmasses.²² They cover the entire wavelength range of the combined atmosphere+CCD response and their construction is described by Fukugita et al. (1996). Also shown in that paper (their Figure 1) are the designed response curves for the filters multiplied by the QE curve of a thinned, UV-AR coated Tektronix TK1024 CCD, similar to the detector that was used in the development of this standard system. The $u'g'r'i'z'$ filters have sharp cutoffs by design. The passbands were selected to exclude the strongest night-sky lines; for example O I ($\lambda 5577$) and Hg I ($\lambda 5461$). The bulk of the u' band response is blueward of the Balmer discontinuity which, when combined with the g' filter, yields high sensitivity to the magnitude of the Balmer jump but at a cost of lower throughput for the narrower u' filter (compared with Johnson U). In Figure 2, we show the filter responses multiplied by the sensitivity data for a CCD similar to that used to set up the $u'g'r'i'z'$ system. These curves represent the expected total quantum efficiencies of the filter transmissions, the QE of the CCD surface, and the reflections from two aluminum mirror surfaces. The two sets of response curves shown are for the case without atmospheric extinction (upper curves) and as modified for typical extinctions at 1.2 airmasses (lower curves). Figure 3 compares the (normalized) $UBVR_cI_c$ filter curves with those of the $u'g'r'i'z'$ system.

The filter transmission data as measured by the Japan Participation Group within the SDSS, the filter manufacturing specifications and the CCD+filter response curves are available on-line at <http://home.fnal.gov/~dtucker/ugriz/index.html>. These curves, as well as the other $u'g'r'i'z'$ links from this page will be updated as needed.

This project used 183 nights of telescope time spanning a 22 month (24 lunation) period beginning in March 1998. The raw statistics for the success of each observing run are in Table 1 where the first two columns give the year and month of the observing session followed by the UT date. The third and fourth columns give the number of nights allocated on the telescope and the number of those nights that were clear, where “clear” is defined as no clouds were seen in the sky by the observer for a stretch greater than three hours at a time. As a consequence, we collected data on some nights indicated as “clear” that later proved not to be usable. The last column gives the total number of usable $u'g'r'i'z'$ observations from each observing run where one observation indicates one star observed once in each of the five filters.

3. The Stars & Observing Strategy

In order to have the standard star system in place for the start of SDSS science operations, as required for follow-up spectroscopy target selection algorithms, it was necessary to save time during

²²Note that the g' filter has been determined to have an effective wavelength 20 Å bluer than that originally quoted by Fukugita et al. (1996).

establishment of the network of standard stars. This was done by making use of previous work on standard stars so that variable stars in the initial fields were already identified. A preliminary list of 63 standard candidates was derived from the work of Thuan & Gunn (1976), Oke & Gunn (1983), and Oke (1990). This list was supplemented using the work of Sandage (1964), Veeder (1974), Stone (1977), and Kent (1985), and then pared to 36 stars using a magnitude cut. The remaining stars were then heavily supplemented using equatorial $UBVR_cI_c$ standard stars (Landolt 1973, 1983, 1992) which served to fill in gaps in right ascension and provide potential color pairs for secondary extinction terms. Additional red stars were obtained from the USNO photometry program (H. Harris, private communication, 1998). At the beginning, our preliminary list contained roughly 200 candidate stars. In the end, the list was trimmed to just those stars with ten or more observations (in each of the five filters) in the current program, or four or more observations in our program provided they had been used as standards in other systems with at least 10 observations to indicate they were not variables. In the end, 164 stars were observed often enough to be included in the reduction process for the final network. Of these, 158 were retained for the final catalog of standards defining the $u'g'r'i'z'$ system.

The primary goals for the SDSS are large scale structure studies using galaxies and QSOs so this first version of the standard network is limited, for the most part, to stars bluer than about M0 to avoid the strengthening metal bands and flare stars. Further, most of the survey area is around the North Celestial Pole with a limited area near the celestial equator, so a heavy emphasis was placed on stars in the northern hemisphere. Expansion of the network to the southern hemisphere and to redder stars is underway (see §6).

Rather than selecting some fiducial spectral type to have null colors (as in the $UBVR_cI_c$ system), our aim was to set the $u'g'r'i'z'$ standard star network on the AB system. Recall that, in the AB system, a monochromatic magnitude is defined such that

$$AB_\nu = -2.5 \log f_\nu - 48.60, \quad (1)$$

where f_ν is the flux per unit frequency from an object in ergs s⁻¹ cm⁻² Hz⁻¹; thus,

$$f_\nu(\text{Jy}) = 3631 \text{ dex}(-0.4AB_\nu) \quad (2)$$

(Oke & Gunn 1983; Fukugita et al. 1996).

As noted, the AB is, strictly speaking, a *monochromatic* system, defining a magnitude for a single frequency ν . The $u'g'r'i'z'$ system, however, is very much a *broadband* filter system. Tying a broadband system to a monochromatic flux is complicated by the existence of stellar absorption lines and by the fact that the mean wavelength of a broadband filter depends on a given star's color. As a compromise solution, we follow Fukugita et al. (1996)'s lead, and define an AB *broadband* magnitude by the following equation:

$$m = -2.5 \log \frac{\int d(\log \nu) f_\nu S_\nu}{\int d(\log \nu) S_\nu} - 48.60, \quad (3)$$

where f_ν is the energy flux per unit frequency on the atmosphere and S_ν is the system response.

To zeropoint the $u'g'r'i'z'$ system, we used the synthetic AB $u'g'r'i'z'$ magnitudes of the F subdwarf BD+17°4708 as calculated by Fukugita et al. (1996). Using equation 3, Fukugita et al. (1996) computed this star’s AB broadband magnitudes by convolving the $u'g'r'i'z'$ system response (Fig. 2) with the Vega-calibrated spectrophotometry of BD+17°4708. Our observations of BD+17°4708 were then forced to match these synthetic magnitudes and all of the standard stars were scaled to this zeropoint. Thus there is a formally defined relationship between $u'g'r'i'z'$ magnitudes and photon flux.

Initial estimates (Eisenstein, private communication; Finkbeiner, private communication) indicate that the present network deviates from a true AB broadband system by no more than about 10% in u' and z' and 5% in $g'r'i'$. These systematic errors are due to uncertainties in the absolute calibration of the synthetic $u'g'r'i'z'$ magnitudes of BD+17°4708, and include uncertainties:

- in the USNO filter transmissions,
- in the CCD response,
- in the atmospheric correction to the filter curves,
- in the relative calibration of BD+17°4708 to Vega, and
- in the absolute calibration of Vega

Since the deviations from a true AB system are due to zeropoint magnitude offsets in the absolute calibration of BD+17°4708 and not due to linear color shifts within the network of stars itself, future corrections towards a AB system — if warranted — should only entail a small additive constant in the standard star magnitudes in each filter band, once these constants have been well determined.

In practice, during the early stages of this program, we needed more than one star to cover the sky for those times when BD+17°4708 was not visible, so two other F subdwarfs were chosen to be reference stars to supplement BD+17°4708: BD+26°2606 and BD+21°0607 (Table 2). BD+26°2606 has excellent spectrophotometry relative to BD+17°4708, and BD+21°0607 has excellent photometric measurements in the Thuau-Gunn system. Thus, all three of these stars were used as fundamental calibration stars during the setup of the $u'g'r'i'z'$ standard star network. Note, however, that the final system zeropoint is tied solely to the synthetic photometry of BD+17°4708.

At the telescope, we tried to observe one of the three fundamental stars at least every 90 minutes to determine the zero points and judge stability for each night. In addition to the fundamental standards, the target list of primary standards was chosen to maximize the color and airmass ranges for each night. In general, two or three primary fields were observed several times to monitor extinction manually at the telescope over the course of a night. These values were compared with

the “all-sky” extinction values determined later by the reduction software using all observations for the night. Additional fields were also observed in a random order to provide a good color spread near the meridian and at high airmass. We attempted to observe each of these fields two or three times a night with at least one hour between repeated observations. On the next usable night of the same observing run, a different set of manual extinction fields was selected and different primary candidate fields were chosen with some, but not complete, overlap. This method reduces dependence on any particular set of extinction stars. The equatorial fields were generally used for extinction to maximize the airmass range and leverage the effect of the color terms. The sky distribution of the final set of stars is shown in Figure 4.

Finally, typically several additional stars within each candidate field were tagged as “extra” or “monitor” stars. Although these stars were excluded from the $u'g'r'i'z'$ standard star network, they are being calibrated in the $u'g'r'i'z'$ system and, after culling variables, will form the basis of a future catalog of supplementary $u'g'r'i'z'$ standards useful for photometric calibration of data from large-format CCD mosaic imaging cameras (Smith et al. 2002).

4. Reductions

4.1. Software

The reductions for this standard system were performed using the “Monitor Telescope Pipeline” (**MTPPIPE**), a suite of code written in the SDSS software environment (Stoughton 1995; Sergey et al. 1996). For the development of the standard star network, the pipeline reductions for each night occurred in three steps — **preMtFrames**, **mtFrames**, and **excal** — briefly described here. A more detailed description can be found in an upcoming paper (Tucker et al. 2002).

The first package, **preMtFrames**, creates the directory structure for the reduction of a night’s data, including parameter files needed as input for the other three packages, and runs quality assurance tests on the raw data. It identifies the image type (e.g., bias frame, twilight flat, standard field), matches the frame name to a list of approved standard star field names, verifies that a full set of frames ($u'g'r'i'z'$) are present for each field, and creates quality assurance histograms for the bias and flat field frames.

The next package, **mtFrames**, is the image processing portion of the software. This package creates median filtered bias and flat frames, applies them to the images, and then extracts aperture photometry on all objects found in each image. The candidate standard stars are measured in a 24-arcsec diameter aperture. This large size was selected to avoid problems associated with defocussing the brightest stars, required for some of the observations.

The third package, **excal**, takes the output of **mtFrames** and identifies the individual primary candidate and fundamental stars within each field, then calculates the photometric zeropoint and the atmospheric extinction using the instrumental magnitudes for these stars as input. Before the

standard star network was calibrated, we used the candidate primary stars as extinction standards and also solved for their best-fit magnitudes based upon that night’s observations. In this mode of operation, only the three fundamental stars — BD+17°4708, BD+26°2606 and BD+21°0607 — had fixed magnitudes; observations of one or more of these three set the photometric zeropoint for the night.

Two additional `mtpipe` packages — `solve_network` and `superExcal` — were used for the final calibration of the primary standard star network. These are similar to `excal` in that they solve for the photometric parameters of a set of data and for the best-fit magnitudes of the primary standards. They differ from `excal` in that they use a single star — BD+17°4708 — to set the zeropoint for the photometric solution. BD+17°4708 is *defined* to have the magnitudes given in Table 2 and sets the zeropoint for the SDSS standard star network. Although both `solve_network` and `superExcal` perform a similar task, they differ from each other in that `superExcal` is largely an outgrowth of the code in `excal` and its least squares solver, but generalized to run on multiple nights of data; `solve_network`, however, was written completely independently of the `excal` code by one of us (MWR). As such, `solve_network` has provided a useful independent check of our `superExcal` results.

To calibrate the standard stars, we took the following steps:

1. We ran `preMtFrames`, `mtFrames`, and `excal` on each night of data from the USNO 1.0-m telescope.
2. From the output of `excal` and from observer notes at the telescope, we determined which nights were photometric.
3. Using the output of `mtFrames` and `excal`, we ran `superExcal` for the final version of the calibrations.
4. Using the output of `mtFrames` and `excal`, we ran the `solve_network` code as an independent check of our `superExcal` results.
5. Finally, we applied a small (0.00–0.04mag) red leak correction to the $u' - g'$ colors, to remove the effects of the u' filter red leaks (see §4.3).

4.2. The Photometric Equations

The equations used to recover the $u'g'r'i'z'$ system have the form:

$$u'_{\text{inst}} = u'_o + a_u + b_u(u' - g')_o + k_u X + c_u[(u' - g')_o - (u' - g')_{o,zp}][X - X_{\text{zp}}] , \quad (4)$$

$$g'_{\text{inst}} = g'_o + a_g + b_g(g' - r')_o + k_g X + c_g[(g' - r')_o - (g' - r')_{o,zp}][X - X_{\text{zp}}] , \quad (5)$$

$$r'_{\text{inst}} = r'_o + a_r + b_r(r' - i')_o + k_r X + c_r[(r' - i')_o - (r' - i')_{o,zp}][X - X_{\text{zp}}] , \quad (6)$$

$$i'_{\text{inst}} = i'_o + a_i + b_i(i' - z')_o + k_i X + c_i[(i' - z')_o - (i' - z')_{o,zp}][X - X_{zp}], \quad (7)$$

$$z'_{\text{inst}} = z'_o + a_z + b_z(i' - z')_o + k_z X + c_z[(i' - z')_o - (i' - z')_{o,zp}][X - X_{zp}]. \quad (8)$$

Taking the g' equation as an example, we note that g'_{inst} is the measured instrumental magnitude, g'_o is the extra-atmospheric magnitude, $(g' - r')_o$ is the extra-atmospheric color, a_g is the nightly zero point, k_g is the first order extinction coefficient, b_g is the system transform coefficient, and c_g is the second order (color) extinction coefficient. The airmass of observation, X , is as defined by Bemporad (1904).

The zeropoint constants, X_{zp} and $(g' - r')_{o,zp}$, used in the second order extinction term, were defined, respectively, to be the average standard star observation airmass $\langle X \rangle = 1.3$ and the “cosmic color,” as listed in Table 3. The cosmic color values were derived from 4428 objects with $19 < r' < 20$ in SDSS survey run 752, camera column 3, fields 11-100 [see Gunn et al. (1998) for a description of the SDSS survey camera]. This area is on the celestial equator at a Galactic latitude of about 42° . The use of these zeropoint constants permits setting c_g to zero without affecting the values of the other terms in the photometric equation (a_g , b_g , and k_g), thus simplifying the photometric equations for projects not requiring the highest photometric accuracy.

The `excal` and `superExcal` packages solve each of the photometric equations (eqs. 4–8) iteratively, performing the following loop:

1. Feed into the equations the current estimates for the extra-atmospheric magnitudes, colors, and photometric coefficients (e.g., for eq. 5, g'_o , r'_o , a_g , b_g , c_g , and k_g). For the first iteration of this loop, initial estimates for these parameters are fed into the equations.
2. Solve each of the equations in turn for the extra-atmospheric magnitude and the non-color-dependent coefficients (e.g., g'_o , a_g , and k_g), keeping the color-dependent coefficients (e.g., b_g , c_g) fixed.
3. Solve each of the equations in turn for the two color-dependent coefficients (e.g., b_g , c_g), keeping the extra-atmospheric magnitude and the non-color-dependent coefficients fixed (e.g., g'_o , a_g , and k_g).
4. Permit the user to delete (or undelete) outliers interactively.

This loop will be performed as long as the user continues to delete (or undelete) observations interactively from the solution. (To ensure that the user has finished modifying the dataset, this loop will run an additional three times after the last user modification before outputting the final photometric solutions.)

One can also choose to fix any of the photometric coefficients to a pre-set value and *not* solve for it. For instance, in setting up the standard star network, we chose to fix the system transform coefficients (e.g., b_g in eq. 5) to zero, since the USNO 1.0-m, its CCD, and its filters are the defining instruments of the $u'g'r'i'z'$ system.

Finally, we note that equations 4–8, which are fit by `excal` and `superExcal`, take the standard magnitudes and colors and convert them to instrumental magnitudes. The inverse equations are:

$$\begin{aligned} u'_o &= u'_{\text{inst}} + \hat{a}_u(u' - g')_{\text{inst}} + \hat{k}_u X \\ &+ \hat{c}_u[(u' - g')_{\text{inst}} - (u' - g')_{\text{inst,zp}}][X - X_{\text{zp}}], \end{aligned} \quad (9)$$

$$\begin{aligned} g'_o &= g'_{\text{inst}} + \hat{a}_g + \hat{b}_g(g' - r')_{\text{inst}} + \hat{k}_g X \\ &+ \hat{c}_g[(g' - r')_{\text{inst}} - (g' - r')_{\text{inst,zp}}][X - X_{\text{zp}}], \end{aligned} \quad (10)$$

$$\begin{aligned} r'_o &= r'_{\text{inst}} + \hat{a}_r + \hat{b}_r(r' - i')_{\text{inst}} + \hat{k}_r X \\ &+ \hat{c}_r[(r' - i')_{\text{inst}} - (r' - i')_{\text{inst,zp}}][X - X_{\text{zp}}], \end{aligned} \quad (11)$$

$$\begin{aligned} i'_o &= i'_{\text{inst}} + \hat{a}_i + \hat{b}_i(i' - z')_{\text{inst}} + \hat{k}_i X \\ &+ \hat{c}_i[(i' - z')_{\text{inst}} - (i' - z')_{\text{inst,zp}}][X - X_{\text{zp}}], \end{aligned} \quad (12)$$

$$\begin{aligned} z'_o &= z'_{\text{inst}} + \hat{a}_z + \hat{b}_z(z' - i')_{\text{inst}} + \hat{k}_z X \\ &+ \hat{c}_z[(i' - z')_{\text{inst}} - (i' - z')_{\text{inst,zp}}][X - X_{\text{zp}}]. \end{aligned} \quad (13)$$

Note that the inverse coefficients have carets, indicating that they do not necessarily have the same values as the direct coefficients of equations 4–8. For a filter x with filter y as its color index conjugate — i.e., filter x 's color index is $(x - y)$ — the conversions from *direct* to *inverse* coefficients are

$$\hat{a}_x = a_x - b_x(a_x - a_y), \quad (14)$$

$$\hat{b}_x = b_x, \quad (15)$$

$$\hat{c}_x = c_x, \quad (16)$$

$$\hat{k}_x = k_x - b_x(k_x - k_y). \quad (17)$$

Again, using the SDSS g' filter as a concrete example,

$$\hat{a}_g = a_g - b_g(a_g - a_r), \quad (18)$$

$$\hat{b}_g = b_g, \quad (19)$$

$$\hat{c}_g = c_g, \quad (20)$$

$$\hat{k}_g = k_g - b_g(k_g - k_r). \quad (21)$$

Furthermore, we note that for the *inverse* equations, we must use an instrumental form of the color zeropoint in the second order extinction term. Again, for a generic filter x with color index $(x - y)$,

$$(x' - y')_{\text{inst,zp}} = (x' - y')_{\text{o,zp}} + (a_x - a_y) + (k_x - k_y)X, \quad (22)$$

and, for our concrete example,

$$(g' - r')_{\text{inst,zp}} = (g' - r')_{\text{o,zp}} + (a_g - a_r) + (k_g - k_r)X. \quad (23)$$

4.3. The Red Leak Correction

There are two small red leaks associated with the u' filter — one at 8120 Å and another, larger leak beyond 10,000 Å. The latter red leak is largely suppressed by the USNO 1.0-m CCD’s low quantum efficiency at these near-infrared wavelengths.

If we define a flux sensitivity quantity, Q , by

$$Q \equiv \int d(\ln \nu) S_\nu, \quad (24)$$

where ν is the frequency and S_ν is the system quantum efficiency (Fukugita et al. 1996, eq. 5), we can calculate the effects of the two red leaks relative to a non-red-leak u' passband. Measured for an airmass of 1.2, we find for the non-red-leak u' passband, the 8120 Å red leak, and the >10,000 Å red leak, respectively:

$$\begin{aligned} Q_{u'} &= 1.842 \times 10^{-2} \\ Q_1 &= 1.009 \times 10^{-6} \\ Q_2 &= 0.783 \times 10^{-7} \end{aligned} \quad (25)$$

The effect of these red leaks in magnitudes can then be calculated by

$$\Delta_i = -2.5 \log(Q_i/Q_{u'}), \quad (26)$$

where $i = 1$ or 2 . We find:

$$\begin{aligned} \Delta_1 &= 10.654 \\ \Delta_2 &= 10.929 \end{aligned} \quad (27)$$

Combining these results, we can calculate the correction we need to apply to an arbitrary $u' - x'$ color of a star (where x' is an arbitrary filter) to remove the effects of these two red leaks:

$$\begin{aligned} (u' - x')_{\text{true}} &= (u' - x')_{\text{obs}} \\ &+ 2.5 \log(1 + 0.4 \text{ dex}[(u' - i')_{\text{true}} - \Delta_1] + 0.4 \text{ dex}[(u' - z')_{\text{true}} - \Delta_2]), \end{aligned} \quad (28)$$

where $(u' - x')_{\text{obs}}$ is $(u' - x')$ before the red leak correction and $(u' - x')_{\text{true}}$ is $(u' - x')$ after the red leak correction. Note that $(u' - i')_{\text{true}}$ and $(u' - z')_{\text{true}}$ are merely $(u' - x')_{\text{true}}$ for $x' = i'$ and $x' = z'$, respectively.

Note that equation 28 is an implicit equation and must be solved iteratively. Fortunately, for cases like ours in which the red leak correction is small, we can use the following approximation:

$$\begin{aligned} (u' - x')_{\text{true}} &= (u' - x')_{\text{obs}} \\ &+ 1.086 \times (\text{dex}[0.4((u' - i')_{\text{obs}} - \Delta_1)] + \text{dex}[0.4((u' - z')_{\text{obs}} - \Delta_2)]), \end{aligned} \quad (29)$$

where we were able to replace $(u' - i')_{\text{true}}$ with $(u' - i')_{\text{obs}}$ and $(u' - z')_{\text{true}}$ with $(u' - z')_{\text{obs}}$ due to the smallness of the red leak corrections. In § 5, where we present the magnitudes and colors for the $u'g'r'i'z'$ primary standards, we use equation 29 to correct the $u' - g'$ colors.

4.4. Data

Both `excal` and `superExcal` solve for first order extinction coefficients that vary over the course of the night; the extinction is determined for individual segments of time called “solution time-blocks.” The first order extinction coefficients for each night used in the `superExcal` photometric solution are given in Table 4. These are arranged by UT date and block (YYMMDD-B) with the corresponding Modified Julian Date for the midpoint of each solution time-block (mid-mjd), rounded to the nearest 0.01 day.²³ These are listed in the first two columns of the table. The extinction coefficients and associated uncertainties are given in columns 3–7. These values were determined as part of the `superExcal` solution. The default solution block within `superExcal` was set at 3 hours. Each night was examined for obvious breaks — east vs. west; the moon; breaks around possible clouds; before and after midnight — and these were given priority for dividing the night into reduction blocks. In the absence of obvious breaks, the default solution block within `MTPPIPE`, 3 hours, was used. Further, each block had to contain a minimum of 10 observations per passband (about 1.5 hours of observing time), after all rejections, to be kept in the final solution. In the end, 109 usable blocks on 61 nights were determined to be photometric and contained the minimum number of observations to be included in the system solution.

The zeropoints for each of the 61 usable nights are shown in Figure 5. These are calculated by `superExcal` once for each block of time, from fundamental standard observations. As shown, most nights have similar zero points. Clearly seen in the figure are the times when the mirrors were re-aluminized: once after the second month and again prior to the last four months of observations. A few outlying points correspond with high extinction values but the derived magnitudes for these nights are within the 2σ error limits for stars observed on those nights.

The primary extinction coefficients (Table 4) for each block are plotted in Figure 6. As seen, the extinction values were generally stable during the program. Three nights with higher than normal extinction values (and low zero points) are seen. However, as mentioned above, the final magnitude values for each of the stars observed during these times were within the accepted limits.

Secondary extinction (color term) values are given in Table 5. Calculating these values is an option in the pipeline code. For the system setup, we assumed there would be one fixed value for all nights and solved for these coefficients. This correction is minor compared with the primary extinction terms so our assumption of a single value does not impact the solution. (For comparison, we also list the values for the secondary extinction coefficients obtained by `solve_network`.)

The residuals of each observation in the network solution were examined for trends, as a function of several different variables, within the final network solution. The plots of these test results are available on our $u'g'r'i'z'$ web site <http://home.fnal.gov/~dtucker/ugriz/index.html>. To summarize, we found no apparent trends in the residuals as a function of:

²³The Modified Julian Date is defined by the relation $\text{MJD} \equiv \text{JD} - 2400000.5$, where JD is the Julian Date.

- time (over the course of the program),
- airmass,
- magnitude,
- color,
- product of color times airmass,
- right ascension,
- declination,
- hour angle,
- ambient temperature of observation.

We did see an increase in the scatter of the residuals in the u' filter at fainter magnitudes and for redder stars. This was caused by the tailored exposure times used on each field with multiple candidate stars. Since the exposure times for each standard field were tailored for the brightest candidate, the second, third, fourth ... star in each field will be increasingly under-exposed resulting in the scatter. We also noticed an increase in scatter for the bluer star residuals in the z' filter; also an artifact of the tailored exposure lengths.

The above tests — those showing the residuals from individual observations plotted against a variety of variables — were useful in showing that there are no obvious systematic trends in the $u'g'r'i'z'$ primary standard star network. To examine the system-wide rms errors in the network, we have plotted the standard error of the mean magnitude for each star in Figures 7 and 8. We have also listed the minimum, the average, and the maximum of these “per star” errors in Table 6, along with the goals needed to meet the survey end-to-end requirements. Figure 7 shows the mean error as a function of magnitude. We clearly see in this plot that the fainter standards in each multiple star field, generally the equatorial fields, have higher errors. Figure 8 shows the mean error as a function of color. Again, we see an increase in the error for the fainter stars in each multiple star field only this time the errors increase for the red stars in the u' frames and the blue stars in the z' frames. In both of these plots, the horizontal dashed lines indicate the survey error budget allotted to the standard star network (the survey goals from Table 6). Note, that, for all but a handful of stars in u' and z' , we more than satisfy the survey goals.

The distribution of the stars in RA- $(g' - r')$ color space is shown in Figure 9. While this plot was generally used as an observation planning tool during system development, it does show the generally uniform distribution of the standards around the sky, at least in the northern hemisphere.

The color-color space distributions of the final set of stars are shown in Figure 10 ($u' - g'$)-vs.-($g' - r'$); Figure 11 ($g' - r'$)-vs.-($r' - i'$); and Figure 12 ($r' - i'$)-vs.-($i' - z'$). The break in the

linear color transforms at about spectral type M0 is clearly seen in Figure 11 and is also evident in Figure 12. Separation of the metal-poor stars from the main sequence dwarfs is seen in Figure 10. The clump of stars in the blue-blue corner of all three of these plots are the warm-hot white dwarfs.

Approximate relations for transforming magnitudes and colors from the Johnson–Morgan–Cousins $UBVR_cI_c$ system to the SDSS $u'g'r'i'z'$ system were given in the system defining paper (Fukugita et al. 1996). Full details of the development of the relations presented herein are given by Jorgensen et al. (2002). Fukugita et al. (1996)’s synthetic transformations and our observed relationships are given in Table 7. Our observed transformation relationships are also shown in graphical form in Figure 13, and are similar to those of Fukugita et al. (1996) (their Figure 6). We also present relations for the inverse transformations — from $u'g'r'i'z'$ to $UBVR_cI_c$ — in Table 7 and in Figure 14.

5. The Standard Star Network

Finally, we present the magnitude and color data for each star along with astrometric, proper motion and spectroscopic information. Table 8 is arranged in order of increasing right ascension and contains the star name, RA and declination (J2000) in the first three columns. The next five columns give the r' magnitudes and the four color indices. (N.B.: the $u' - g'$ colors listed here have had the u' red leak correction of eq. 29 applied; see Fig. 15.) These five columns are linked with the next five columns (9–13) which give the standard deviation of the measurements. As a note, during the reductions we calculated the five filter magnitudes. We report colors here as an observational aid. The associated uncertainties for the colors are derived from the magnitude errors added in quadrature. As such, they may be slightly overestimated. The last five columns of this table give the number of individual measurements, by filter, that were used to determine the final magnitudes.

Table 9 is arranged by increasing RA and the first three columns are the same as Table 8. Column 4 gives the Guide Star or Hipparcos catalog number, or indicates it is in the Tycho database. The coordinate epoch follows in column 5. Columns 6–10 give the proper motions and uncertainties in milli-arcsec yr^{-1} and the reference where these were obtained. Columns 11 and 12 give the spectral type (where known) and reference. The last column indicates that additional notes on a star may be found in the footnotes to the table.

6. Future Work

Though the setup of the initial primary standard stars for the $u'g'r'i'z'$ system is now complete, there is still a large amount of work remaining to make this system widely useful to the astronomical community. Two efforts which will continue through the life of the SDSS are reducing the errors in the mean magnitudes of each standard star and obtaining good magnitudes for all of the additional

stars in each of the standard star fields. These will be done by making use of the observations of the SDSS photometric monitoring telescope at Apache Point Observatory. This telescope operates every night during survey operations to obtain extinction data for survey calibration and to transfer the standard star system, through fainter stars, to the 2.5-m survey data.

In addition to the continued refinement of the primary standard star network, two additional areas which require more work are extending the system to redder stars and to the southern hemisphere. The initial standard system was limited to stars generally bluer than about dM0, so the redder stars are needed to obtain accurate magnitudes for the late M dwarfs and the new spectral classes, L and T. An extension to redder stars will make the logical tie into the 2MASS survey for the redder objects more meaningful. We are developing a program to make this extension, specifically to look for additional “knees” in the color–color diagrams. The second area of expansion is into the southern hemisphere. We began this effort in September 2000 using the 0.9-m at CTIO and the same observers and reduction software as used in the setup of the network described in this present paper²⁴. We undertook this effort to minimize any discrepancies such as those which have crept into the existing $UBVR_cI_c$ standards, in which several independent investigators have been involved in calibrating standard stars.

The Sloan Digital Sky Survey is a joint project of The University of Chicago, Fermilab, the Institute for Advanced Study, the Japan Participation Group, The Johns Hopkins University, the Max-Plank-Institute for Astronomy (MPIA), the Max-Plank-Institute for Astrophysics (MPA), the New Mexico State University, Princeton University, the United States Naval Observatory, and the University of Washington. Apache Point Observatory, site of the SDSS telescopes, is operated by the Astrophysicsal Research Consortium (ARC).

Funding for the project has been provided by the Alfred P. Sloan Foundation, the SDSS member institutions, the National Aeronautics and Space Administration, the National Science Foundation, the U.S. Department of Energy, the Japanese Monbukagakusho, and the Max Planck Society. The official SDSS Web site is <http://www.sdss.org>.

The authors would like to thank the USNO-Flagstaff for making the telescope and detector available for the observations; and Conard Dahn, Joe Hobart, Fred Harris and Hugh Harris for their assistance during the observing sessions. We also thank David Hogg, Michael Strauss, and Gillian Knapp for their valuable reading of the manuscript and comments. JAS also acknowledges the many useful discussions of the project with Conard Dahn and Hugh Harris at USNO, Arlo Landolt at LSU, and Brian Skiff at Lowell Observatory. JAS further acknowledges Lowell Observatory for its support and hospitality during the observing runs. JAS and DLT acknowledge Jeanne Odermann and Sahar Allam for their help in proofreading the text. Finally, we acknowledge the referee,

²⁴http://home.fnal.gov/~dtucker/Southern_ugriz/index.html

B. Oke, for his many insightful suggestions which have substantially improved the quality of the paper and presentation of the data.

This research has made use of the SIMBAD database, operated at CDS, Strasbourg, France.

REFERENCES

- Bemporad, A. 1904, Mitteil. Grossherzogl. Sternwarte, Heidelberg, 4
- Berger, J., & Fringant, A. M. 1980, A&A, 85, 367 (BH80)
- Bidelman, W. P. 1985, ApJS, 59, 197 (B85)
- Cannon, A. J., & Pickering, E. C. 1918–24, Henry Draper Catalogue and Extension, Harv. Ann. 91–100 (HD)
- Carney, B. W. 1983, AJ, 88, 610 (C83)
- Carney, B. W., & Latham, D. W. 1987, AJ, 93, 116 (CL87)
- Cowley, A. P., Hiltner, W. A., & Witt, A. N. 1967, AJ, 72, 1334 (CH67)
- Doyle, J. G., & Butler, C. J. 1990, A&A, 235, 335 (DB90)
- Drilling, J. S., & Landolt, A. U. 1979, AJ, 84, 783 (DL79)
- Duquennoy, A., & Mayor, M. 1991, A&A, 248, 485 (DM91)
- Eggen, O. J., & Sandage, A. 1959, MNRAS, 119, 255 (ES59)
- Elkin, V. G. 1996, A&A, 312L, 5 (E96)
- Fukugita, M., Ichikawa, T., Gunn, J. E., Doi, M., Shimasaku, K., & Schneider, D. P. 1996, AJ, 111, 1748
- Giclas, H. L., Burnham, R., Jr., & Thomas, N. G. 1978, Lowell Proper Motion Survey, Southern Hemisphere Catalog, Lowell Observatory Bulletin, No. 164, 8, 89 (G78)
- Gizis, J. E. 1997, AJ, 113, 806 (G97)
- Greenstein, J. L. 1954, PASP, 66, 126 (G54)
- Greenstein, J. L. 1984, ApJ, 276, 602 (G84)
- Greenstein, J. L., & Sargent, A. I. 1974, ApJS, 28, 157 (GS74)
- Gunn, J. E., Carr, M., Rockosi, C., Sekiguchi, M., et al. 1998, AJ, 116, 3040
- Harrington, R. S., & Dahn, C. C. 1980, AJ, 85, 454 (HD80)
- Heintz, W. D. 1993, AJ, 105, 1188 (He93)
- Heintz, W. D. 1994, AJ, 108, 2338 (He94)
- Henry, T. J., Kirkpatrick, J. D., & Simons, D. A. 1994, AJ, 108, 1437 (HK94)

- Hiltner, W. A. 1956, ApJS, 2, 389 (H56)
- Holberg, J. B, Bastrow, M. A., & Sion, E. M. 1998, ApJS, 119, 207 (HBS98)
- Høg, E., Fabricius, C., Makarov, V. V. et al. 2000, A&A, 355, L27 (TYC2)
- Houk, N., & Smith-Moore, M. 1988, Michigan Catalogue of Two-Dimensional Spectral Types for the HD Stars, Vol. 4, Univ. of Michigan, Ann Arbor (MSS88)
- Houk, N., & Swift, C. 1999, Michigan Catalogue of Two-Dimensional Spectral Types for the HD Stars, Vol. 5, Univ. of Michigan, Ann Arbor (MSS99)
- Iriarte, B. 1958, ApJ, 127, 507 (Ir58)
- Jones, D. H. P. 1966, R. Obs. Bull. No. 126 (J66)
- Johnson, H. L., & Morgan, W. W. 1953, ApJ, 117, 313 (JM53)
- Jorgensen, A., et al. 2002, in preparation
- Kent, S. 1985, PASP, 97, 165
- Landolt, A. U. 1973, AJ, 78, 959 (L73)
- Landolt, A. U. 1983, AJ, 88, 439
- Landolt, A. U. 1992, AJ, 104, 372
- Lasker, B. M., Russel, J. N., & Jenkner, H. 1996–99, The Guide Star Catalog Version 1.1-ACT (GSC-ACT Catalogue), The Association of Universities for Research in Astronomy, Inc. (GSC)
- Little, J. E., Dufton, P. L., Keenan, F. P., Hambly, N. C., Conlon, E. S., Brown, P. J. F., & Miller, L. 1995, ApJ, 447, 783 (LD95)
- Luyten, W. J. 1979, New Luyten Catalogue of Stars with Proper Motions Larger than Two Tenths of an Arcsecond Vol 1 & 2, Univ. of Minnesota, Minneapolis + Vol. 3 & 4 (1980) (NLTT)
- McCook, G. P., & Sion, E. M. 1987, ApJS, 65, 603 (GE87)
- McCook, G. P. & Sion, E. M. 1999, ApJS, 121, 1 (MS99)
- Mermilliod, J.-C., Mermilliod, M., & Hauck, B. 1997, A&AS, 124, 349
- Oke, J. B. 1990, AJ, 99, 1621
- Oke, J. B., & Gunn, J. E. 1983, ApJ, 266, 713

- Perryman, M. A. C. & ESA 1997, The Hipparcos and Tycho catalogues. Astrometric and photometric star catalogues derived from the ESA Hipparcos Space Astrometry Mission, Publisher: Noordwijk, Netherlands: ESA Publications Division, 1997, Series: ESA SP Series vol no: 1200, ISBN: 9290923997 (set) (HIP, TYC1)
- Popper, D. 1942, ApJ, 95, 307 (P42)
- Popper, D. 1943, ApJ, 98, 209 (P43)
- Reid, I. N., Hawley, S. L., & Gizis, J. E. 1995, AJ, 110, 1838 (MSU)
- Roman, N. G. 1955, ApJS, 2, 195 (Ro55)
- Sandage, A. 1964, ApJ, 139, 442
- Sandage, A. 1969, ApJ, 158, 1115 (S69)
- Sergey, G., Berman, E., Huang, C.-H., Kent, S., Newberg, H., Nicinski, T., Petrvick, D., & Stoughton, C. 1996, in Astronomical Data Analysis Software and Systems V, ASP Conf. Ser., Vol. 101, ed. G. H. Jacoby & J. Barnes, (San Francisco:ASP), 248
- Smith, J. A., et al. 2002, in preparation
- Smithsonian Astrophysical Observatory Staff 1966, United States Naval Observatory, Astronomical Data Center 1990, SAO Star Catalog J2000 (SAO)
- Stone, R. P. S. 1977, ApJ, 218, 767
- Stone, R. P. S. 1996, ApJS, 107, 423 (S96)
- Stoughton, C. 1995, BAAS, 187, 9101
- Stoughton, C., Lupton, R. H., Bernardi, M. et al. 2001, AJ, in press
- Thejll, P. 1997, A&A, 317, 689 (TF97)
- Thuan, T. X., & Gunn, J. E. 1976, PASP, 88, 543
- Tucker, D. L., et al. 2002, in preparation
- Turnshek, D. A., Bohlin, R. C., Williamson, R. L., II, Lupie, O. L., & Koornneef, J. 1990, AJ, 99, 1243 (T90)
- van Altena, W., Lee, J. T., & Hoffleit, D., The General Catalogue of Trigonometric (Stellar) Parallaxes, Fourth Edition, 1995, Yale University, New Haven (YTP95)
- Veeder, G. J. 1974, AJ, 79, 1056
- Weis, E. W. 1994, AJ, 107, 1135 (W94)

York, D. G., Adelman, J., Anderson, J. E. et al. 2000, AJ, 120, 1579

Table 1. Observing Runs at USNO 1.0-m Telescope

YYMM	UT Dates	Nights	Clear ^a	# Obs.
9803	03/11–03/16	6	2	91
9804	04/10–04/17	8	2	78
9805	05/09–05/18	10	5	213
9806	06/06–06/14	9	6	236
9807	07/07–07/13	7	1	45
9808	08/05–08/11	7	0	0
9809	09/02–09/10	9	0	0
9810	10/02–10/08	7	3	126
9811	10/29–11/09	11	5	195
9812	11/28–12/04	7	3	70
9901	12/31–01/05	6	3	140
9902	01/27–02/04	9	6	212
9903	02/27–03/05	7	2	92
9904	03/27–04/04	9	3	130
9905	04/26–05/03	8	3	58
9905	05/27–05/31	5	0	0
9906	06/26–07/02	7	5	183
9907	07/23–07/28	6	0	0
9908	08/24–08/30	7	0	0
9909	09/22–09/28	7	4	228
9910	10/20–10/28	9	6	215
9911	11/18–11/25	8	2	97
9912	12/17–12/23	7	3	116
0001	01/21–01/27	7	0	0
Σ		183	64	2525

^aHere, a “clear” night is as judged at the telescope.

Table 2. The $u'g'r'i'z'$ Fundamental Standards

Star ^a	R.A.	Dec.	u'	g'	r'	i'	z'
BD+17°4708	22:11:30	+18:05:30	10.56	9.64	9.35	9.25	9.23
BD+26°2606	14:49:02	+25:42:27	10.761	9.891	9.604	9.503	9.486
σ			0.001	0.001	0.001	0.001	0.001
BD+21°0607	04:14:35	+22:21:06	10.289	9.395	9.114	9.025	9.017
σ			0.002	0.001	0.001	0.001	0.001

^aThe magnitudes for BD+17°4708 are defined as given in this table.

Table 3. The Cosmic Colors

color	value	scatter
$(u' - g')$	1.42	± 0.82
$(g' - r')$	1.11	± 0.46
$(r' - i')$	0.48	± 0.34
$(i' - z')$	0.35	± 0.22

Table 4. First Order Extinction Coefficients

Date-B	mid-mjd	$k_{u'}$	$\sigma_{u'}$	$k_{g'}$	$\sigma_{g'}$	$k_{r'}$	$\sigma_{r'}$	$k_{i'}$	$\sigma_{i'}$	$k_{z'}$	$\sigma_{z'}$
980311-0	50883.22	0.565	0.018	0.161	0.007	0.102	0.006	0.062	0.007	0.050	0.011
980311-1	50883.42	0.554	0.024	0.166	0.009	0.108	0.008	0.060	0.009	0.049	0.015
980316-0	50888.27	0.594	0.013	0.182	0.004	0.092	0.004	0.071	0.006	0.051	0.009
980316-1	50888.44	0.617	0.017	0.188	0.007	0.105	0.006	0.075	0.007	0.071	0.012
980411-0	50914.21	0.619	0.014	0.205	0.005	0.116	0.004	0.082	0.006	0.064	0.010
980411-1	50914.41	0.587	0.013	0.201	0.005	0.113	0.004	0.080	0.006	0.065	0.010
980417-0	50920.42	0.569	0.040	0.192	0.015	0.116	0.013	0.066	0.014	0.072	0.023
980510-0	50943.24	0.769	0.017	0.264	0.007	0.177	0.006	0.149	0.007	0.167	0.010
980510-1	50943.41	0.726	0.017	0.293	0.006	0.212	0.005	0.167	0.007	0.171	0.011
980511-0	50944.21	0.654	0.022	0.273	0.010	0.153	0.008	0.110	0.010	0.127	0.013
980511-1	50944.31	0.616	0.022	0.319	0.010	0.255	0.010	0.093	0.009	0.112	0.012
980511-2	50944.43	0.682	0.022	0.236	0.008	0.158	0.007	0.099	0.009	0.113	0.014
980515-0	50948.39	0.568	0.019	0.180	0.007	0.104	0.007	0.075	0.008	0.076	0.012
980516-0	50949.21	0.592	0.022	0.196	0.008	0.112	0.007	0.071	0.008	0.068	0.013
980516-1	50949.36	0.592	0.024	0.189	0.009	0.117	0.008	0.076	0.009	0.078	0.014
980517-0	50950.27	0.656	0.031	0.187	0.008	0.123	0.007	0.082	0.008	0.036	0.013
980517-1	50950.40	0.526	0.031	0.168	0.012	0.108	0.011	0.072	0.011	0.067	0.017
980606-0	50970.34	0.571	0.017	0.198	0.006	0.132	0.005	0.095	0.008	0.105	0.012
980607-0	50971.23	0.565	0.019	0.184	0.006	0.110	0.005	0.085	0.007	0.086	0.011
980607-1	50971.38	0.585	0.018	0.180	0.007	0.117	0.006	0.094	0.008	0.073	0.012
980608-0	50972.22	0.589	0.018	0.201	0.006	0.107	0.006	0.059	0.007	0.052	0.011
980608-1	50972.38	0.582	0.015	0.202	0.006	0.127	0.005	0.094	0.007	0.091	0.010
980609-0	50973.29	0.505	0.027	0.202	0.010	0.125	0.009	0.111	0.012	0.095	0.018
980610-0	50974.23	0.597	0.019	0.207	0.008	0.134	0.007	0.086	0.008	0.092	0.012
980610-1	50974.39	0.609	0.017	0.209	0.007	0.137	0.006	0.119	0.007	0.102	0.012
980614-0	50978.24	0.596	0.018	0.207	0.007	0.132	0.006	0.091	0.008	0.089	0.012
980614-1	50978.40	0.569	0.018	0.166	0.007	0.098	0.006	0.078	0.007	0.073	0.011
980713-0	51007.22	0.566	0.029	0.191	0.009	0.130	0.007	0.074	0.009	0.067	0.014
980713-1	51007.37	0.609	0.015	0.192	0.005	0.108	0.005	0.086	0.007	0.073	0.010
981003-0	51089.16	0.546	0.023	0.165	0.008	0.102	0.007	0.064	0.009	0.057	0.014
981003-1	51089.37	0.525	0.023	0.165	0.009	0.107	0.008	0.068	0.010	0.069	0.015
981006-0	51092.20	0.572	0.017	0.169	0.006	0.088	0.006	0.059	0.007	0.066	0.011
981006-1	51092.42	0.555	0.015	0.171	0.006	0.106	0.005	0.063	0.007	0.056	0.010
981007-0	51093.26	0.548	0.025	0.152	0.008	0.085	0.007	0.055	0.009	0.078	0.013
981102-0	51119.44	0.562	0.017	0.180	0.006	0.105	0.005	0.069	0.007	0.069	0.011
981103-0	51120.42	0.544	0.015	0.160	0.005	0.097	0.005	0.067	0.006	0.077	0.010
981104-0	51121.14	0.532	0.017	0.164	0.006	0.091	0.006	0.065	0.007	0.064	0.011
981104-1	51121.30	0.551	0.016	0.165	0.006	0.093	0.005	0.062	0.007	0.061	0.011
981104-2	51121.46	0.509	0.020	0.162	0.008	0.099	0.007	0.056	0.008	0.065	0.013
981105-0	51122.27	0.611	0.016	0.194	0.007	0.100	0.006	0.143	0.008	0.118	0.012
981105-1	51122.45	0.559	0.029	0.169	0.011	0.090	0.010	0.068	0.011	0.078	0.017
981106-0	51123.16	0.544	0.021	0.163	0.008	0.094	0.007	0.062	0.008	0.069	0.012

Table 4—Continued

Date-B	mid-mjd	$k_{u'}$	$\sigma_{u'}$	$k_{g'}$	$\sigma_{g'}$	$k_{r'}$	$\sigma_{r'}$	$k_{i'}$	$\sigma_{i'}$	$k_{z'}$	$\sigma_{z'}$
981106-1	51123.45	0.566	0.016	0.161	0.006	0.099	0.005	0.053	0.007	0.051	0.011
981130-0	51147.42	0.495	0.018	0.150	0.007	0.082	0.006	0.061	0.008	0.058	0.012
981201-0	51148.46	0.510	0.023	0.145	0.008	0.076	0.007	0.051	0.009	0.053	0.014
981201-0	51149.49	0.549	0.028	0.165	0.010	0.103	0.009	0.076	0.011	0.074	0.017
981202-1	51149.12	0.568	0.022	0.152	0.008	0.077	0.008	0.046	0.008	0.072	0.013
990103-0	51181.24	0.527	0.019	0.172	0.006	0.092	0.006	0.071	0.007	0.047	0.011
990103-1	51181.46	0.524	0.021	0.173	0.007	0.111	0.006	0.055	0.008	0.018	0.012
990104-0	51182.14	0.587	0.015	0.162	0.006	0.091	0.005	0.064	0.007	0.044	0.010
990104-1	51182.30	0.581	0.025	0.162	0.008	0.097	0.008	0.054	0.008	0.052	0.014
990104-2	51182.49	0.625	0.029	0.156	0.011	0.087	0.025	0.063	0.011	0.056	0.016
990105-0	51183.26	0.577	0.019	0.170	0.007	0.081	0.006	0.049	0.007	0.064	0.011
990129-0	51207.14	0.551	0.019	0.146	0.007	0.093	0.006	0.048	0.008	0.041	0.012
990129-1	51207.36	0.513	0.019	0.163	0.007	0.085	0.006	0.038	0.008	0.028	0.012
990130-0	51208.15	0.542	0.019	0.186	0.007	0.106	0.007	0.064	0.008	0.058	0.012
990131-0	51209.12	0.556	0.019	0.153	0.007	0.080	0.006	0.062	0.008	0.048	0.012
990201-0	51210.20	0.541	0.015	0.170	0.005	0.107	0.004	0.070	0.006	0.061	0.010
990202-0	51211.22	0.548	0.014	0.166	0.005	0.092	0.005	0.050	0.006	0.046	0.010
990202-1	51211.47	0.518	0.028	0.178	0.011	0.105	0.009	0.069	0.010	0.056	0.016
990203-0	51212.18	0.516	0.021	0.151	0.008	0.082	0.007	0.046	0.008	0.051	0.013
990302-0	51239.21	0.557	0.016	0.177	0.006	0.125	0.006	0.079	0.007	0.068	0.010
990302-1	51239.43	0.542	0.016	0.173	0.006	0.103	0.005	0.079	0.007	0.061	0.011
990303-0	51240.44	0.535	0.017	0.166	0.006	0.093	0.006	0.060	0.007	0.047	0.011
990328-0	51265.16	0.696	0.022	0.241	0.008	0.156	0.007	0.100	0.008	0.104	0.012
990328-1	51265.35	0.622	0.020	0.221	0.007	0.143	0.007	0.098	0.008	0.104	0.012
990329-0	51266.17	0.740	0.023	0.258	0.009	0.175	0.007	0.113	0.008	0.121	0.012
990329-1	51266.38	0.802	0.019	0.375	0.006	0.253	0.005	0.174	0.007	0.157	0.011
990331-0	51268.22	1.160	0.023	0.575	0.010	0.403	0.008	0.323	0.009	0.232	0.013
990331-1	51268.43	0.735	0.022	0.305	0.008	0.203	0.007	0.147	0.009	0.100	0.014
990502-0	51300.30	0.620	0.017	0.212	0.006	0.129	0.008	0.100	0.007	0.109	0.011
990502-1	51300.42	0.608	0.033	0.223	0.013	0.143	0.010	0.099	0.012	0.068	0.019
990627-0	51356.22	0.601	0.021	0.179	0.007	0.116	0.007	0.090	0.008	0.109	0.012
990627-1	51356.39	0.610	0.015	0.176	0.006	0.114	0.005	0.089	0.007	0.105	0.011
990629-0	51358.24	0.583	0.016	0.205	0.006	0.119	0.006	0.091	0.007	0.107	0.011
990629-1	51358.41	0.557	0.017	0.139	0.006	0.099	0.006	0.045	0.007	0.047	0.011
990630-0	51359.23	0.561	0.024	0.189	0.009	0.118	0.008	0.088	0.009	0.074	0.014
990630-1	51359.40	0.572	0.019	0.179	0.007	0.115	0.007	0.087	0.008	0.076	0.012
990701-0	51360.23	0.637	0.017	0.204	0.006	0.132	0.006	0.095	0.007	0.107	0.011
990701-1	51360.39	0.634	0.017	0.197	0.006	0.129	0.006	0.094	0.007	0.097	0.011
990925-0	51446.27	0.584	0.016	0.162	0.006	0.098	0.005	0.077	0.007	0.091	0.010
990925-1	51446.45	0.590	0.016	0.176	0.006	0.110	0.005	0.091	0.007	0.099	0.010
990926-0	51447.16	0.562	0.016	0.178	0.006	0.094	0.005	0.072	0.007	0.076	0.010
990926-1	51447.31	0.546	0.022	0.174	0.009	0.087	0.008	0.056	0.009	0.073	0.014

Table 4—Continued

Date-B	mid-mjd	$k_{u'}$	$\sigma_{u'}$	$k_{g'}$	$\sigma_{g'}$	$k_{r'}$	$\sigma_{r'}$	$k_{i'}$	$\sigma_{i'}$	$k_{z'}$	$\sigma_{z'}$
990926-2	51447.45	0.554	0.016	0.158	0.006	0.082	0.005	0.063	0.007	0.062	0.011
990927-0	51448.17	0.553	0.016	0.164	0.006	0.093	0.005	0.061	0.007	0.059	0.011
990927-1	51448.32	0.589	0.020	0.170	0.008	0.106	0.007	0.075	0.008	0.099	0.012
990927-2	51448.45	0.550	0.017	0.178	0.006	0.107	0.006	0.071	0.007	0.086	0.011
990928-0	51449.18	0.583	0.016	0.180	0.006	0.108	0.006	0.076	0.007	0.087	0.011
990928-1	51449.42	0.557	0.017	0.173	0.006	0.084	0.006	0.074	0.007	0.078	0.011
991020-0	51471.20	0.539	0.043	0.166	0.016	0.086	0.014	0.065	0.016	0.092	0.024
991020-1	51471.44	0.578	0.020	0.166	0.006	0.093	0.005	0.063	0.007	0.057	0.011
991021-0	51472.17	0.591	0.014	0.182	0.006	0.110	0.004	0.077	0.006	0.081	0.010
991021-1	51472.34	0.604	0.020	0.167	0.008	0.098	0.007	0.061	0.008	0.053	0.013
991022-0	51473.12	0.557	0.021	0.167	0.008	0.100	0.007	0.068	0.008	0.055	0.013
991022-1	51473.48	0.569	0.031	0.153	0.012	0.095	0.010	0.072	0.012	0.050	0.018
991023-0	51474.14	0.546	0.018	0.167	0.007	0.094	0.006	0.056	0.007	0.047	0.011
991023-1	51474.30	0.581	0.020	0.174	0.008	0.097	0.007	0.065	0.008	0.067	0.012
991025-0	51476.47	0.591	0.026	0.168	0.009	0.099	0.008	0.071	0.010	0.084	0.015
991026-0	51477.16	0.702	0.028	0.210	0.011	0.121	0.010	0.069	0.011	0.061	0.016
991026-1	51477.30	0.617	0.019	0.194	0.008	0.105	0.007	0.067	0.008	0.067	0.012
991026-2	51477.46	0.673	0.022	0.222	0.008	0.136	0.007	0.086	0.009	0.080	0.013
991121-0	51503.38	0.549	0.016	0.157	0.005	0.094	0.005	0.060	0.007	0.061	0.010
991123-0	51505.20	0.569	0.017	0.180	0.006	0.105	0.006	0.056	0.007	0.025	0.012
991123-1	51505.45	0.530	0.021	0.164	0.008	0.096	0.007	0.060	0.009	0.029	0.013
991221-0	51533.16	0.526	0.014	0.157	0.005	0.087	0.005	0.054	0.006	0.064	0.010
991221-1	51533.37	0.577	0.019	0.175	0.007	0.104	0.006	0.064	0.008	0.062	0.013
991222-0	51534.49	0.591	0.022	0.200	0.009	0.122	0.008	0.085	0.009	0.074	0.014
991223-0	51535.14	0.585	0.023	0.153	0.009	0.109	0.008	0.067	0.009	0.063	0.015
991223-1	51535.31	0.536	0.018	0.164	0.007	0.090	0.006	0.070	0.008	0.079	0.011

Table 5. Second Order Extinction Coefficients

Filter	superExcal	solve_network
$c_{u'}$	-0.021 ± 0.003	-0.032
$c_{g'}$	-0.016 ± 0.003	-0.015
$c_{r'}$	-0.004 ± 0.003	$+0.000$
$c_{i'}$	$+0.006 \pm 0.003$	$+0.005$
$c_{z'}$	$+0.003 \pm 0.003$	$+0.006$

Table 6. Mean Errors in Calibrated Magnitudes

Filter	Survey Goal	Calculated		
		minimum	average	maximum
$\sigma_{u'}$	0.015	0.001	0.007	0.025
$\sigma_{g'}$	0.010	0.001	0.002	0.006
$\sigma_{r'}$	0.010	0.001	0.002	0.008
$\sigma_{i'}$	0.010	0.001	0.002	0.009
$\sigma_{z'}$	0.015	0.001	0.003	0.016

Table 7. Transformations Between $UBVR_cI_c$ and $u'g'r'i'z'$

Mag/Color	Observed	Synthetic ^a
$UBVR_cI_c \longrightarrow u'g'r'i'z'$		
g'	$= V + 0.54(B - V) - 0.07$	$= V + 0.56(B - V) - 0.12$
r'	$= V - 0.44(B - V) + 0.12$	$= V - 0.49(B - V) + 0.11$
r' for $(V - R) < 1.00$	$= V - 0.81(V - R) + 0.13$	$= V - 0.84(V - R) + 0.13$
r' for $(V - R) \geq 1.00$...	$= V - 0.84(V - R) + 0.13$
$u' - g'$	$= 1.33(U - B) + 1.12$	$= 1.38(U - B) + 1.14$
$g' - r'$	$= 0.98(B - V) - 0.19$	$= 1.05(B - V) - 0.23$
$r' - i'$ for $(R - I) < 1.15$	$= 1.00(R - I) - 0.21$	$= 0.98(R - I) - 0.23$
$r' - i'$ for $(R - I) \geq 1.15$	$= 1.42(R - I) - 0.69$	$= 1.40(R - I) - 0.72$
$r' - z'$ for $(R - I) < 1.65$	$= 1.65(R - I) - 0.38$	$= 1.59(R - I) - 0.40$
$r' - z'$ for $(R - I) \geq 1.65$	none observed	$= 2.64(R - I) - 2.16$
$u'g'r'i'z' \longrightarrow UBVR_cI_c$		
B	$= g' + 0.47(g' - r') + 0.17$...
V	$= g' - 0.55(g' - r') - 0.03$...
$U - B$	$= 0.75(u' - g') - 0.83$...
$B - V$	$= 1.02(g' - r') + 0.20$...
$V - R$	$= 0.59(g' - r') + 0.11$...
$R - I$ for $(r' - i') < 0.95$	$= 1.00(r' - i') + 0.21$...
$R - I$ for $(r' - i') \geq 0.95$	$= 0.70(r' - i') + 0.49$...

^aFrom Fukugita et al. (1996).

Table 8—Continued

Star Name	RA (J2000.0)	DEC (J2000.0)	r'	$u' - g'$	$g' - r'$	$r' - i'$	$i' - z'$	$\sigma_{r'}$	$\sigma_{u' - g'}$	$\sigma_{g' - r'}$	$\sigma_{r' - i'}$	$\sigma_{i' - z'}$	$n_{u'}$	$n_{g'}$	$n_{r'}$	$n_{i'}$	$n_{z'}$
Ru 149B	07:24:17.53	-00:33:05.4	12.474	1.385	0.460	0.141	0.033	0.001	0.006	0.002	0.001	0.002	36	40	40	40	39
LHS 0033	07:27:24.49	+05:13:32.9	9.286	2.839	1.331	1.477	0.695	0.002	0.005	0.003	0.004	0.006	13	13	13	9	9
Ru 152	07:29:58.44	-02:06:37.5	13.188	-0.263	-0.355	-0.289	-0.252	0.002	0.005	0.004	0.005	0.007	9	9	9	9	5
SA 99 438	07:55:54.26	-00:16:49.1	9.569	0.136	-0.348	-0.293	-0.220	0.002	0.006	0.004	0.003	0.003	12	12	13	14	14
SA 99 447	07:56:06.68	-00:20:42.3	9.572	0.734	-0.287	-0.245	-0.161	0.003	0.005	0.004	0.004	0.003	13	13	14	16	16
BD+75 0325	08:10:49.50	+74:57:57.8	9.786	-0.508	-0.514	-0.382	-0.323	0.002	0.005	0.004	0.003	0.004	14	13	14	14	14
BD+8 2015	08:15:41.62	+07:37:05.9	10.194	1.393	0.497	0.173	0.065	0.002	0.005	0.003	0.002	0.003	21	20	21	20	21
BD+54 1216	08:19:22.56	+54:05:09.7	9.586	0.890	0.300	0.107	0.010	0.001	0.004	0.002	0.002	0.004	17	16	17	16	16
GCRV 5757	08:44:05.00	+36:14:43.9	10.803	1.000	0.403	0.152	0.048	0.001	0.004	0.002	0.002	0.003	13	13	13	13	13
BD+25 1981	08:44:24.68	+24:47:47.9	9.270	0.925	0.144	0.014	-0.037	0.002	0.004	0.003	0.003	0.004	19	19	19	18	19
SA 100 241	08:52:34.05	-00:39:48.8	10.204	1.165	-0.068	-0.128	-0.097	0.003	0.005	0.004	0.004	0.004	13	12	12	13	12
SA 100 280	08:53:35.47	-00:36:41.0	11.689	1.143	0.308	0.084	0.003	0.002	0.006	0.003	0.003	0.004	15	15	17	16	16
SA 100 394	08:53:54.51	-00:32:22.0	10.932	2.979	1.056	0.419	0.237	0.001	0.015	0.002	0.001	0.001	10	15	17	16	15
GCRV 5951	09:05:16.68	+38:47:54.7	11.474	0.854	0.346	0.135	0.029	0.002	0.004	0.004	0.003	0.004	11	11	11	11	11
PG0918+029D	09:21:21.94	+02:47:28.7	11.937	2.227	0.817	0.324	0.166	0.002	0.010	0.003	0.003	0.004	17	18	18	18	19
BD+9 2190	09:29:15.55	+08:38:00.6	11.049	0.902	0.238	0.076	0.009	0.001	0.006	0.002	0.001	0.002	10	11	11	10	10
BD-12 2918	09:31:19.42	-13:29:19.3	9.476	2.817	1.326	1.201	0.561	0.002	0.005	0.003	0.004	0.004	11	11	12	10	11
Ross 889	09:40:43.19	+01:00:29.5	10.380	0.875	0.220	0.068	0.006	0.002	0.004	0.004	0.003	0.004	7	8	7	7	8
SA 101 315	09:54:51.28	-00:27:31.1	10.894	2.490	0.894	0.350	0.196	0.002	0.006	0.002	0.003	0.003	24	24	25	24	24
SA 101 316	09:54:52.03	-00:18:34.4	11.438	1.152	0.309	0.073	0.007	0.001	0.005	0.001	0.001	0.003	24	24	24	24	24
SA 101 207	09:57:52.48	-00:47:36.4	12.290	1.085	0.347	0.101	0.022	0.002	0.005	0.003	0.004	0.004	11	11	10	11	11
G 162-66	10:33:42.81	-11:41:38.7	13.227	-0.183	-0.387	-0.354	-0.303	0.001	0.014	0.005	0.007	0.014	4	4	3	4	4
Feige 34	10:39:36.73	+43:06:09.2	11.423	-0.509	-0.508	-0.347	-0.265	0.002	0.004	0.003	0.002	0.003	16	16	16	16	16
BD+29 2091	10:47:23.16	+28:23:56.0	10.123	0.864	0.366	0.132	0.040	0.006	0.012	0.008	0.008	0.006	9	9	8	8	9
PG1047+003A	10:50:05.65	-00:01:11.3	13.303	1.385	0.519	0.212	0.087	0.003	0.009	0.004	0.004	0.005	15	20	21	20	20
Ross 106	10:50:28.98	+56:26:31.0	12.413	1.028	0.434	0.176	0.060	0.003	0.008	0.004	0.004	0.006	10	10	9	10	10
SA 102 620	10:55:04.22	-00:48:18.9	9.665	2.464	0.932	0.309	0.148	0.002	0.009	0.003	0.004	0.004	11	11	9	11	11
G 163 50	11:07:59.97	-05:09:26.0	13.266	0.215	-0.277	-0.272	-0.271	0.003	0.004	0.004	0.004	0.007	16	16	16	16	14
G 163 51	11:08:06.55	-05:13:46.9	11.960	2.741	1.315	1.238	0.567	0.003	0.014	0.004	0.004	0.004	8	17	17	12	12
Wolf 365	11:11:00.00	+06:25:11.3	11.135	1.182	0.560	0.237	0.097	0.003	0.007	0.004	0.004	0.005	12	12	11	13	13
GCRV 7017	11:32:23.31	+76:39:18.1	11.326	1.120	0.517	0.212	0.080	0.003	0.006	0.005	0.004	0.005	12	12	12	12	12
BD-21 3420	11:55:28.45	-22:23:13.3	10.021	0.998	0.322	0.122	0.036	0.008	0.010	0.009	0.012	0.011	8	6	5	8	8
SA 103 626	11:56:46.14	-00:23:14.6	11.753	1.056	0.246	0.056	-0.027	0.003	0.009	0.004	0.004	0.006	15	15	14	16	13
SA 103 526	11:56:54.18	-00:30:13.5	10.575	2.434	0.826	0.293	0.164	0.002	0.011	0.004	0.003	0.004	10	17	14	16	16
Ross 453	12:10:55.77	+00:23:54.3	10.971	0.872	0.298	0.101	0.025	0.005	0.009	0.006	0.006	0.006	12	10	11	13	13
Feige 66	12:37:23.52	+25:03:59.9	10.747	-0.345	-0.476	-0.367	-0.316	0.002	0.003	0.002	0.002	0.004	15	16	17	16	16
SA 104 428	12:41:41.31	-00:26:26.5	12.330	2.153	0.763	0.279	0.147	0.002	0.008	0.004	0.004	0.005	7	11	12	12	11
SA 104 598	12:45:16.78	-00:16:40.4	11.057	2.481	0.985	0.339	0.148	0.005	0.015	0.006	0.006	0.006	8	9	9	11	10
Ross 484	13:18:56.71	-03:04:18.0	10.378	2.000	0.855	0.327	0.165	0.003	0.009	0.004	0.004	0.006	8	9	9	9	9
LTT 5137	13:20:23.67	-03:01:41.8	11.190	1.103	0.455	0.181	0.063	0.004	0.011	0.006	0.005	0.007	7	6	6	6	7
GCRV 7951	13:21:47.60	+74:12:32.9	11.488	0.876	0.341	0.134	0.035	0.001	0.005	0.002	0.001	0.003	11	12	12	12	12
PG1323-086D	13:26:05.26	-08:50:35.7	11.928	1.210	0.397	0.132	0.032	0.001	0.003	0.001	0.001	0.002	22	21	23	23	22
G 14-55	13:28:21.09	-02:21:36.7	10.633	2.813	1.325	1.333	0.615	0.002	0.007	0.004	0.003	0.004	13	13	13	12	13
BD+30 2428B	13:37:13.80	+30:05:14.2	10.239	1.844	0.668	0.223	0.107	0.003	0.006	0.004	0.004	0.004	10	10	10	10	10
SA 105 815	13:40:02.50	-00:02:18.8	11.366	0.863	0.232	0.076	0.003	0.002	0.005	0.003	0.004	0.005	13	13	13	13	13
BD+2 2711	13:42:19.01	+01:30:18.6	10.548	0.166	-0.362	-0.301	-0.234	0.002	0.005	0.004	0.004	0.005	10	10	10	10	10
HD 121968	13:58:51.17	-02:54:52.3	10.425	-0.064	-0.370	-0.318	-0.245	0.003	0.005	0.004	0.004	0.005	5	6	6	6	5
Ross 838	14:01:44.47	+08:55:17.4	11.327	1.277	0.573	0.239	0.111	0.002	0.007	0.003	0.003	0.004	17	17	17	16	16
BD+26 2606	14:49:02.35	+25:42:09.2	9.604	0.870	0.287	0.101	0.017	0.001	0.001	0.001	0.001	0.001	122	125	124	126	125
GCRV 8758	15:07:41.38	+32:24:37.2	10.954	1.258	0.492	0.176	0.062	0.002	0.004	0.003	0.003	0.004	15	15	15	15	15
PG1528+062B	15:30:39.55	+06:01:13.1	11.828	1.235	0.419	0.143	0.036	0.001	0.004	0.001	0.001	0.002	32	33	33	33	33

Table 8—Continued

Star Name	RA (J2000.0)	DEC (J2000.0)	r'	$u' - g'$	$g' - r'$	$r' - i'$	$i' - z'$	$\sigma_{r'}$	$\sigma_{u' - g'}$	$\sigma_{g' - r'}$	$\sigma_{r' - i'}$	$\sigma_{i' - z'}$	$n_{u'}$	$n_{g'}$	$n_{r'}$	$n_{i'}$	$n_{z'}$
BD+38 4955	23:13:38.81	+39:25:02.6	10.800	1.038	0.515	0.220	0.096	0.001	0.005	0.001	0.001	0.002	13	12	13	13	13
BD+33 4737	23:34:36.13	+34:02:22.2	8.840	1.653	0.572	0.177	0.062	0.002	0.004	0.003	0.003	0.003	16	16	16	16	16
PG2336+004B	23:38:38.26	+00:42:46.4	12.312	1.101	0.336	0.100	0.014	0.001	0.007	0.003	0.002	0.005	14	14	14	14	14
SA 115 420	23:42:36.48	+01:05:58.8	11.063	1.091	0.290	0.080	0.007	0.002	0.004	0.003	0.002	0.003	18	19	19	19	18
SA 115 516	23:44:15.38	+01:14:12.5	10.107	2.167	0.807	0.317	0.172	0.002	0.009	0.004	0.003	0.004	16	16	16	16	16

Table 9. The $u'g'r'i'z'$ standard star network: astrometry, spectral properties, and notes.

Star Name	α (J2000.0)	δ (J2000.0)	T-Tycho/GSC/Hipp #	Epoch year	$\mu(\alpha \cos \delta)$ marcsec/yr	$\sigma(\mu(\alpha \cos \delta))$ marcsec/yr	$\mu(\delta)$ marcsec/yr	$\sigma(\mu(\delta))$ marcsec/yr	pm ref.	spectral type	spectrum ref.	Notes
Hilt 31	00:28:11.15	+64:07:51.8		T 2000.000	-3.90	3.40	-4.90	3.50	TYC2	B1V	H56	1
G 158-100	00:33:54.60	-12:07:58.9	G0527100531	2000.000	152.00	3.00	-179.00	4.00	HD80	DG	G84	w,2
BD+71 0031	00:43:44.34	+72:10:43.1		3430 2000.000	321.50	1.80	90.70	1.80	TYC2	sdF5	C83	m
SA 92 342	00:55:09.90	+00:43:12.9		T 2000.000	-2.20	1.70	-0.20	1.70	TYC2	F5	DL79	
SA 92 263	00:55:39.41	+00:36:20.0	G0001200675	1983.702	N/A	G8III	DL79	
SA 92 502	00:56:08.13	+01:04:25.1		T 2000.000	7.20	1.70	7.40	1.70	TYC2	N/A	N/A	
SA 92 282	00:56:46.86	+00:38:30.9		T 2000.000	28.30	2.80	6.10	2.70	TYC2	A5	DL79	
SA 92 288	00:57:17.00	+00:36:48.7		T 2000.000	4.90	1.40	4.90	1.40	TYC2	K3V	DL79	
SA 93 317	01:54:37.73	+00:43:00.5		T 2000.000	-9.30	1.60	-18.50	1.70	TYC2	F5	DL79	
SA 93 333	01:55:05.22	+00:45:42.5		T 2000.000	18.60	1.70	-1.80	2.00	TYC2	G5	DL79	
SA 93 424	01:55:26.35	+00:56:42.5		T 2000.000	3.70	1.70	-3.40	1.90	TYC2	G8III	DL79	
Hilt 190	01:58:24.07	+61:53:43.5		T 2000.000	-6.40	2.90	-1.60	2.90	TYC2	B1V:	H56	
LHS 0014	02:12:20.99	+03:34:32.4		10279 2000.000	-1761.70	1.60	-1851.70	1.60	TYC2	M1.5	MSU	m
Hilt 233	02:12:29.97	+59:54:04.1		T 2000.000	3.30	3.60	-3.80	3.70	TYC2	O9V	H56	3
Feige 22	02:30:16.62	+05:15:50.6		11650 2000.000	71.15	6.60	-24.60	4.20	HIP	DA3	GE87	4
SA 94 242	02:57:21.24	+00:18:38.9	G0004801015	1983.703	N/A	A2	MSU	
SA 94 251	02:57:46.98	+00:16:02.7	G0004801221	1983.703	N/A	K1III	DL79	
SA 94 702	02:58:13.37	+01:10:54.3	G0004800918	1983.703	N/A	K2:	DL79	
Ross 374	03:26:59.76	+23:46:35.9		16072 2000.000	262.70	1.50	-348.60	1.50	HIP	F5	B85	m
Ross 34	03:28:53.14	+37:22:56.7		16209 2000.000	1120.24	2.70	-1065.81	2.70	HIP	sdK7	G97	m
SA 95 96	03:52:54.18	+00:00:18.7		T 2000.000	13.80	0.90	-1.60	0.90	TYC2	A0	DL79	
SA 95 190	03:53:13.24	+00:16:22.8		T 2000.000	-1.90	1.90	-1.00	2.00	TYC2	N/A	N/A	
SA 95 193	03:53:20.59	+00:16:34.7	G0006600670	1984.729	N/A	N/A	N/A	
Hilt 404	03:53:59.42	+53:12:56.8		T 2000.000	-3.40	2.20	1.20	2.10	TYC2	B1V	H56	
SA 95 218	03:54:49.95	+00:10:08.5	G0006600856	1984.729	N/A	G2V	DL79	
SA 95 132	03:54:51.67	+00:05:21.5		T 2000.000	-4.90	2.30	-9.90	2.40	TYC2	A4	DL79	
SA 95 142	03:55:09.40	+00:01:20.6	G0006600917	1984.729	N/A	N/A	N/A	
SA 95 149	03:55:44.44	+00:07:02.8		T 2000.000	21.30	2.10	-19.80	2.10	TYC2	G9IV	DL79	
SA 95 236	03:56:13.34	+00:08:47.0		T 2000.000	15.60	2.20	40.70	2.20	TYC2	G5IV	DL79	
BD+21 0607	04:14:35.51	+22:21:04.3		19797 2000.000	427.30	0.90	-303.40	0.90	TYC2	sdF5	C83	m
BD-21 0910	04:33:16.19	-21:08:07.1		21232 2000.000	-32.20	1.60	-185.90	1.60	TYC2	G5V	MSS88	m
SA 96 36	04:51:42.40	-00:10:09.4		T 2000.000	-13.90	1.20	-1.80	1.20	TYC2	A2	DL79	
SA 96 737	04:52:35.34	+00:22:30.2	G0008500158	1983.774	N/A	K0	Simbad	5
SA 96 83	04:52:58.86	-00:14:41.3		T 2000.000	0.30	1.30	-3.20	1.30	TYC2	A3	DL79	
SA 96 235	04:53:18.87	-00:05:01.6		T 2000.000	3.00	1.50	0.70	1.50	TYC2	G9III	DL79	
Ross 49	05:44:56.81	+09:14:32.2		27111 2000.000	86.80	2.50	-634.80	2.50	TYC2	F8:	B85	6
SA 97 249	05:57:07.56	+00:01:11.6		T 2000.000	19.30	1.70	2.40	1.70	TYC2	G5V	DL79	
SA 97 345	05:57:33.16	+00:21:16.4	G0011700815	1983.848	N/A	G8III:	DL79	
SA 97 351	05:57:37.30	+00:13:44.0		T 2000.000	1.30	1.20	-0.80	1.10	TYC2	AO	DL79	
SA 97 75	05:57:55.08	-00:09:28.5		T 1991.850	N/A	K5:	DL79	
SA 97 284	05:58:25.02	+00:05:13.5		T 2000.000	0.30	1.50	-4.40	1.50	TYC2	G8III	DL79	7
SA 97 288	05:58:30.09	+00:06:40.7		T 2000.000	0.40	1.90	-15.20	1.90	TYC2	G0	DL79	
Hilt 566	06:32:09.67	+03:34:44.4		T 2000.000	4.00	1.70	0.90	1.80	TYC2	F5	HD	8
LHS 1858	06:37:10.80	+17:33:53.3		31635 2000.000	-765.40	1.60	338.10	1.50	TYC2	dM1	W94	m,9
SA 98 978	06:51:33.72	-00:11:31.5		T 2000.000	25.20	1.30	-29.60	1.30	TYC2	G3V	DL79	
SA 98 185	06:52:01.88	-00:27:21.6		T 2000.000	1.00	1.20	0.10	1.20	TYC2	A2	DL79	
SA 98 193	06:52:03.37	-00:27:18.3		T 2000.000	2.80	1.20	-10.90	1.20	TYC2	K1III	DL79	
SA 98 653	06:52:04.94	-00:18:18.2		T 2000.000	-0.30	1.10	-3.50	1.10	TYC2	B9	DL79	
SA 98 685	06:52:18.46	-00:20:19.5		T 2000.000	-0.60	2.50	-2.80	2.70	TYC2	F8	DL79	

Table 9—Continued

Star Name	α (J2000.0)	δ (J2000.0)	T-Tycho/GSC/Hipp	Epoch #	year	$\mu(\alpha \cos \delta)$ marcsec/yr	$\sigma(\mu(\alpha \cos \delta))$ marcsec/yr	$\mu(\delta)$ marcsec/yr	$\sigma(\mu(\delta))$ marcsec/yr	pm ref.	spectral type	spectrum ref.	Notes
Ru 149F	07:24:14.02	-00:31:38.2	G0481700748	1982.895	N/A	N/A	N/A	
Ru 149D	07:24:15.36	-00:32:47.9		T	2000.000	-2.40	1.50	-1.80	1.50	TYC2	N/A	N/A	
Ru 149B	07:24:17.53	-00:33:05.4	G0481700990	1982.895	N/A	N/A	N/A	
LHS 0033	07:27:24.49	+05:13:32.9		36208	2000.000	573.60	2.40	-3691.00	2.30	TYC2	M3.5V	HK94	m,10
Ru 152	07:29:58.44	-02:06:37.5	G0482100403	1982.895	N/A	O5V	T90	p
SA 99 438	07:55:54.26	-00:16:49.1		T	2000.000	-19.20	0.90	17.20	1.00	TYC2	B2	DL79	11
SA 99 447	07:56:06.68	-00:20:42.3		T	2000.000	-9.90	1.00	-4.50	1.00	TYC2	B8	DL79	12
BD+75 0325	08:10:49.50	+74:57:57.8		40047	2000.000	9.10	1.10	10.60	1.20	TYC2	sdOp	BH80	
BD+8 2015	08:15:41.62	+07:37:05.9		T	2000.000	-223.00	4.60	-157.00	4.50	TYC1	A2	SAO	13
BD+54 1216	08:19:22.56	+54:05:09.7		40778	2000.000	-35.80	1.30	-625.90	1.40	TYC2	sdF6	CH67	m
GCRV 5757	08:44:05.00	+36:14:43.9		42864	2000.000	-22.40	3.60	-457.70	3.30	TYC2	sdF8	P43	14
BD+25 1981	08:44:24.68	+24:47:47.9		42887	2000.000	-112.60	1.30	-348.40	1.20	TYC2	sdF2	S69	
SA 100 241	08:52:34.05	-00:39:48.8		T	2000.000	1.00	1.20	-2.10	1.10	TYC2	A3	DL79	
SA 100 280	08:53:35.47	-00:36:41.0		T	2000.000	11.20	2.10	-8.40	2.10	TYC2	F8	DL79	
SA 100 394	08:53:54.51	-00:32:22.0		T	2000.000	-2.80	2.00	2.00	2.00	TYC2	K2III:	DL79	
GCRV 5951	09:05:16.68	+38:47:54.7		44605	2000.000	4.60	2.30	-471.20	2.20	TYC2	sdF5	P43	m
PG0918+029D	09:21:21.94	+02:47:28.7		T	1982.878	N/A	N/A	N/A	
BD+9 2190	09:29:15.55	+08:38:00.6		46516	2000.000	199.00	1.80	-307.80	1.70	TYC2	sdA5	ES59	
BD-12 2918	09:31:19.42	-13:29:19.3		46706	2000.000	730.30	1.60	23.10	1.60	TYC2	M3	MSU	15
Ross 889	09:40:43.19	+01:00:29.5		T	2000.000	148.20	1.50	-508.60	1.50	TYC2	sdA4	P43	16
SA 101 315	09:54:51.28	-00:27:31.1		T	2000.000	-3.70	1.80	-1.50	1.90	TYC2	K0III	DL79	
SA 101 316	09:54:52.03	-00:18:34.4		T	2000.000	2.80	1.80	-10.60	1.80	TYC2	F6	DL79	
SA 101 207	09:57:52.48	-00:47:36.4		T	2000.000	-4.30	2.00	4.20	2.00	TYC2	F8	DL79	
G 162-66	10:33:42.81	-11:41:38.7	G0549500166	2000.000	-297.00	30.00	-55.00	30.00	G78	DA2	HBS98	w,17	
Feige 34	10:39:36.73	+43:06:09.2		52181	2000.000	12.00	1.50	-24.90	1.50	TYC2	D0	S96	s,18
BD+29 2091	10:47:23.16	+28:23:56.0		52771	2000.000	179.40	1.40	-824.50	1.40	TYC2	sdG5	C83	m
PG1047+003A	10:50:05.65	-00:01:11.3	G0491400008	1982.368	N/A	N/A	N/A	
Ross 106	10:50:28.98	+56:26:31.0	G0382600684	2000.000	158.00	5.00	-401.00	4.00	NLT	G8:	NLT	m	
SA 102 620	10:55:04.22	-00:48:18.9		53383	2000.000	-235.20	1.20	13.40	1.20	TYC2	M0III	DL79	m
G 163 50	11:07:59.97	-05:09:26.0	G0492700597	2000.000	-38.00	30.00	-426.00	30.00	G78	DA3	GE87	m,w,19	
G 163 51	11:08:06.55	-05:13:46.9	G0492701272	2000.000	-38.00	30.00	-426.00	30.00	G78	M3	MSU	m,20	
Wolf 365	11:11:00.00	+06:25:11.3		54639	2000.000	-568.50	2.20	-517.70	2.10	TYC2	sdG3	P42	m
GCRV 7017	11:32:23.31	+76:39:18.1		56291	2000.000	115.20	2.00	-599.70	2.20	TYC2	sdG0	P42	
BD-21 3420	11:55:28.45	-22:23:13.3		58145	2000.000	-156.40	1.70	-199.80	2.10	TYC2	F50V	SAO	
SA 103 626	11:56:46.14	-00:23:14.6		T	2000.000	15.40	2.40	-6.20	2.50	TYC2	F3	DL79	
SA 103 526	11:56:54.18	-00:30:13.5		T	2000.000	-13.00	1.20	13.90	1.20	TYC2	K0III	DL79	21
Ross 453	12:10:55.77	+00:23:54.3		59376	2000.000	-56.10	1.30	-436.40	1.30	TYC2	sdF2	P43	m
Feige 66	12:37:23.52	+25:03:59.9		61602	2000.000	2.60	1.40	-27.40	1.40	TYC2	sdOB	E96	
SA 104 428	12:41:41.31	-00:26:26.5	G0494900310	1987.330	N/A	N/A	N/A	
SA 104 598	12:45:16.78	-00:16:40.4		T	2000.000	-138.30	1.40	-76.90	1.50	TYC2	K5V	DL79	
Ross 484	13:18:56.71	-03:04:18.0		64965	2000.000	-643.00	4.10	-130.20	4.40	TYC2	dK8.5	DB90	m,22
LTT 5137	13:20:23.67	-03:01:41.8		65081	2000.000	29.70	1.80	-191.80	1.80	TYC2	N/A	N/A	m
GCRV 7951	13:21:47.60	+74:12:32.9		65206	2000.000	-443.90	2.00	40.00	2.10	TYC2	sdF2	YTP95	m
PG1323-086D	13:26:05.26	-08:50:35.7	G0554400406	1983.194	N/A	N/A	N/A	
G 14-55	13:28:21.09	-02:21:36.7		65714	2000.000	153.00	1.70	-491.80	1.80	TYC2	M3	MSU	23
BD+30 2428B	13:37:13.80	+30:05:14.2		66441	2000.000	-158.30	2.40	41.10	2.30	TYC2	K1	MSU	24
SA 105 815	13:40:02.50	-00:02:18.8		66673	2000.000	-226.80	1.50	-83.30	1.50	TYC2	A0	DL79	m,25
BD+2 2711	13:42:19.01	+01:30:18.6		66872	2000.000	-6.10	1.20	0.50	1.20	TYC2	B4V	LD95	m
HD 121968	13:58:51.17	-02:54:52.3		68297	2000.000	1.60	1.10	18.20	1.20	TYC2	B2II	MSS99	

Table 9—Continued

Star Name	α (J2000.0)	δ (J2000.0)	T-Tycho/GSC/Hipp #	Epoch year	$\mu(\alpha \cos \delta)$ marcsec/yr	$\sigma(\mu(\alpha \cos \delta))$ marcsec/yr	$\mu(\delta)$ marcsec/yr	$\sigma(\mu(\delta))$ marcsec/yr	pm ref.	spectral type	spectrum ref.	Notes
Ross 838	14:01:44.47	+08:55:17.4	68527	2000.000	157.40	2.60	-748.20	2.50	TYC2	sdG3	P43	m
BD+26 2606	14:49:02.35	+25:42:09.2	72461	2000.000	-8.50	1.30	-345.50	1.20	TYC2	sdF4	C83	m
GCRV 8758	15:07:41.38	+32:24:37.2	74029	2000.000	-136.00	1.90	-458.70	1.80	TYC2	G6V	CH67	
PG1528+062B	15:30:39.55	+06:01:13.1	T	2000.000	-12.70	2.60	7.20	2.50	TYC2	N/A	N/A	
G 15-24	15:30:41.76	+08:23:40.4	T5946	2000.000	-394.70	2.60	-118.40	2.50	TYC2	G4	J66	
SA 107 1006	15:38:33.37	+00:14:19.2	T	2000.000	25.80	2.50	-22.80	2.50	TYC2	G5V	DL79	
SA 107 351	15:38:45.75	-00:32:06.5	T	2000.000	-12.60	2.20	-7.40	2.20	TYC2	F8	DL79	
BD+33 2642	15:51:59.88	+32:56:54.3	77716	2000.000	-10.10	1.80	3.70	1.90	TYC2	B2IVp	Ir58	p
Ross 530	16:19:51.66	+22:38:20.2	80003	2000.000	-40.27	1.98	-451.15	2.32	HIP	sdG2:	P43	m
GCRV 9483	16:28:16.87	+44:40:38.3	80679	2000.000	-266.90	1.50	-687.20	1.40	TYC2	G5	B85	m
SA 108 475	16:37:00.60	-00:34:39.0	T	2000.000	-0.30	2.00	-0.60	2.10	TYC2	K0III	DL79	
SA 108 551	16:37:47.79	-00:33:05.1	T	2000.000	5.50	1.20	5.10	1.20	TYC2	A0	DL79	
Wolf 629	16:55:25.66	-08:19:13.1	82809	2000.000	-813.43	4.43	-895.17	2.46	HIP	M3.5V	HK94	m,26
BD+18 3407	17:35:19.89	+18:53:00.8	86063	2000.000	71.00	1.10	-314.00	1.10	TYC2	G5	Simbad	
BD+2 3375	17:39:45.59	+02:24:59.6	86443	2000.000	-367.00	1.30	73.80	1.20	TYC2	sdGO	C83	
SA 109 71	17:44:06.78	-00:24:57.8	T	2000.000	-0.60	1.50	0.00	1.50	TYC2	A0	DL79	
SA 109 381	17:44:12.26	-00:20:32.7	T	2000.000	-2.40	1.60	4.00	1.50	TYC2	F2:	DL79	
SA 109 231	17:45:19.95	-00:25:51.6	T	2000.000	2.40	0.80	-14.30	0.90	TYC2	K2II	DL79	
SA 109 537	17:45:42.45	-00:21:35.4	T	2000.000	1.00	1.20	-1.90	1.20	TYC2	F1	DL79	
Hilt 733	18:17:23.32	-11:44:57.5	T	2000.000	-0.70	2.20	-4.30	2.20	TYC2	B1:II:	H56	
Ross 711	18:35:19.17	+28:41:55.3	91129	2000.000	-16.30	1.90	-276.60	1.90	TYC2	sdA7	G54	m,27
SA 110 232	18:40:52.33	+00:01:54.8	T	2000.000	-11.40	2.50	-25.60	2.60	TYC2	N/A	N/A	
SA 110 340	18:41:28.44	+00:15:23.0	T	2000.000	2.70	1.10	-6.90	1.10	TYC2	A5II	MSS99	28
SA 110 499	18:43:07.66	+00:28:01.4	T	2000.000	3.90	1.70	-0.30	1.70	TYC2	B9	DL79	
SA 110 503	18:43:11.69	+00:29:42.9	T	2000.000	3.10	1.60	-6.80	1.60	TYC2	A0	DL79	
GJ 745A	19:07:05.57	+20:53:16.9	93873	2000.000	-473.70	1.60	-350.30	1.60	TYC2	M1.5	MSU	
GJ 745B	19:07:13.19	+20:52:37.2	93899	2000.000	-479.30	1.70	-333.40	1.60	TYC2	M2	MSU	
BD+35 3659	19:31:09.22	+36:09:10.1	95996	2000.000	-9.20	1.90	-563.70	1.90	TYC2	sdF7	Ro55	m
SA 111 775	19:37:16.36	+00:12:05.5	T	2000.000	-2.20	1.60	-6.70	1.70	TYC2	N/A	N/A	
SA 111 1925	19:37:28.62	+00:25:03.1	G0047801393	1983.680	N/A	A0	DL79	
Wolf 1346	20:34:21.89	+25:03:49.7	101516	2000.000	-402.60	1.70	-563.30	1.70	TYC2	DA2.5	HBS98	m,p,w,29
SA 112 223	20:42:14.58	+00:08:59.7	T	2000.000	6.30	1.50	-10.70	1.50	TYC2	F5	DL79	
SA 112 250	20:42:26.38	+00:07:42.4	T	2000.000	1.00	1.60	-9.50	1.70	TYC2	F8	DL79	
SA 112 805	20:42:46.74	+00:16:08.4	G0051101428	1983.683	N/A	A1	DL79	
SA 112 822	20:42:54.90	+00:15:01.9	T	2000.000	-4.50	1.70	-13.20	1.80	TYC2	G8III	DL79	
BD+62 1916	21:15:05.74	+62:50:27.9	104913	2000.000	122.40	2.00	259.50	2.00	TYC2	G5	DM91	m
SA 113 339	21:40:55.64	+00:27:58.2	G0054301300	1983.683	N/A	F8	DL79	
SA 113 466	21:41:27.39	+00:40:15.6	T	2000.000	19.60	1.20	7.90	1.20	TYC2	F5	DL79	
SA 113 259	21:41:44.84	+00:17:39.9	T	1991.600	N/A	K0III	DL79	
SA 113 260	21:41:48.03	+00:23:53.3	G0054301222	1983.683	N/A	N/A	N/A	
SA 113 475	21:41:51.30	+00:39:20.8	T	2000.000	16.50	1.40	-15.20	1.40	TYC2	G9III	DL79	
BD+28 4211	21:51:11.02	+28:51:50.4	107864	2000.000	-36.90	2.00	-56.60	2.00	TYC2	Op	JM53	s,w,30
G 93-48	21:52:25.37	+02:23:19.6	107968	2000.000	14.10	2.10	-300.40	2.10	TYC2	DA3	GE87	s,31
BD+25 4655	21:59:41.96	+26:25:57.3	108578	2000.000	-37.70	1.30	-44.40	1.20	TYC2	sdO0	GS74	32
Hilt 1089	22:09:20.87	+57:51:28.4	T	2000.000	-2.30	2.90	-1.70	2.90	TYC2	B0.5n(V)	H56	
BD+17 4708	22:11:31.37	+18:05:34.1	109558	2000.000	507.20	1.30	57.60	1.3	TYC2	sdF8	Simbad	m
BD-11 5781	22:13:10.68	-11:10:38.4	109695	2000.000	288.60	1.80	-91.90	1.80	TYC2	K1V	MSS99	33
SA 114 531	22:40:36.78	+00:51:55.6	G0056800830	1982.842	N/A	G5	DL79	
SA 114 654	22:41:26.14	+01:10:10.7	T	2000.000	34.00	1.40	-11.80	1.40	TYC2	G0	DL79	

Table 9—Continued

Star Name	α (J2000.0)	δ (J2000.0)	T-Tycho/GSC/Hipp #	Epoch year	$\mu(\alpha \cos \delta)$ marcsec/yr	$\sigma(\mu(\alpha \cos \delta))$ marcsec/yr	$\mu(\delta)$ marcsec/yr	$\sigma(\mu(\delta))$ marcsec/yr	pm ref.	spectral type	spectrum ref.	Notes
SA 114 656	22:41:35.06	+01:11:09.8	G0056801464	1982.842	N/A	N/A	N/A	
SA 114 548	22:41:36.83	+00:59:05.7		T 2000.000	-1.60	2.80	-7.20	3.10	TYC2	K2:	DL79	
SA 114 750	22:41:44.70	+01:12:36.2		T 2000.000	-11.20	1.60	-24.10	1.60	TYC2	B9	DL79	
G 27-45	22:44:56.30	-02:21:12.8	112310	2000.000	738.30	1.80	-243.10	1.90	TYC2	KO	YTP95	m
Ross 786	23:09:33.34	+00:43:02.1		T 2000.000	-258.00	39.00	-1280.00	39.00	TYC1	sdG2	YTP95	m,34
GD 246	23:12:23.07	+10:47:04.2	G0116401078	2000.000	1414.00	34.00	-22.00	34.00	TF97	DA1	HBS98	m,w,35
BD+38 4955	23:13:38.81	+39:25:02.6	114661	2000.000	168.60	3.10	-314.10	3.10	TYC2	sdF0	C83	m
BD+33 4737	23:34:36.13	+34:02:22.2	116351	2000.000	360.60	1.50	166.00	1.50	TYC2	K2	J66	36
PG2336+004B	23:38:38.26	+00:42:46.4	G0058500720	1983.680	N/A	N/A	N/A	
SA 115 420	23:42:36.48	+01:05:58.8		T 2000.000	-7.50	1.60	-3.80	1.60	TYC2	F5	DL79	
SA 115 516	23:44:15.38	+01:14:12.5		T 2000.000	31.80	1.60	-21.30	1.60	TYC2	G8IV	DL79	

^m High proper motion star.

^p HST &/or IUE photometric standard.

^s HST &/or FUV spectrophotometric standard.

^w White dwarf star.

¹ Heavily reddened star.

² Not listed in Villanova WD catalog (MS99); =EGGR-382, LTT-300, G270-8, USNO-490.

³ Blue straggler in Per OB1 association.

⁴ =WD0227+050, EG019.

⁵ The northern star in an optical pair.

⁶ Optical double, separation 0.95'.

⁷ Listed as G5III in Simbad.

⁸ =HD 259211.

⁹ Listed as K7 (MSU); W94 notes as long term variable.

¹⁰ cf. W94 notes as long term variable; dM4; =“Luyten’s Star”.

¹¹ Listed as B2III in Simbad.

¹² Listed as B9V in Simbad.

¹³ The southern star in an optical pair.

¹⁴ Listed as G0 by Kuiper in B85; =LTT12271.

¹⁵ Integrated magnitude and spectral type, separation 0.66'.

¹⁶ The SW star in an optical double (CL87).

¹⁷ =WD1031-114, EG070, LTT3870.

¹⁸ =WD1036+433.

¹⁹ =WD1105-048, LP672-1, EG076, LTT4099, GJ1152B.

²⁰ =LP672-2, GJ1152A.

²¹ Listed as G0III in Simbad.

²² Listed as sdK in G97, sdK4 in P43.

²³ Listed as M4 in MSU; suspected variable; =GL512A.

²⁴ Listed as G8V in Simbad; =Gl-518.2B; western star of optical pair.

²⁵ Listed as A5p in L73.

²⁶ =GJ643.

²⁷ Listed as A8 in Simbad and newer papers.

²⁸ =HD 172652.

²⁹ =WD2032+248, EG139, LTT16005, G186-031, Gl-794, LHS 3562, LFT 1554, AC+25-68981.

³⁰ Listed as DA in Villanova WD catalog (MS99); =WD2148+286.

³¹ =WD2149+021, EG150, Gl-838.4.

³² Low amplitude variable, IS Peg (ZZ Cet type).

³³ Integrated magnitude and spectral type, separation 0.93'.

³⁴ Listed as sdG in G97, G2VI in He94.

³⁵ =WD2309+105, EG233, BPM97895.

³⁶ Listed as K0 in Simbad.

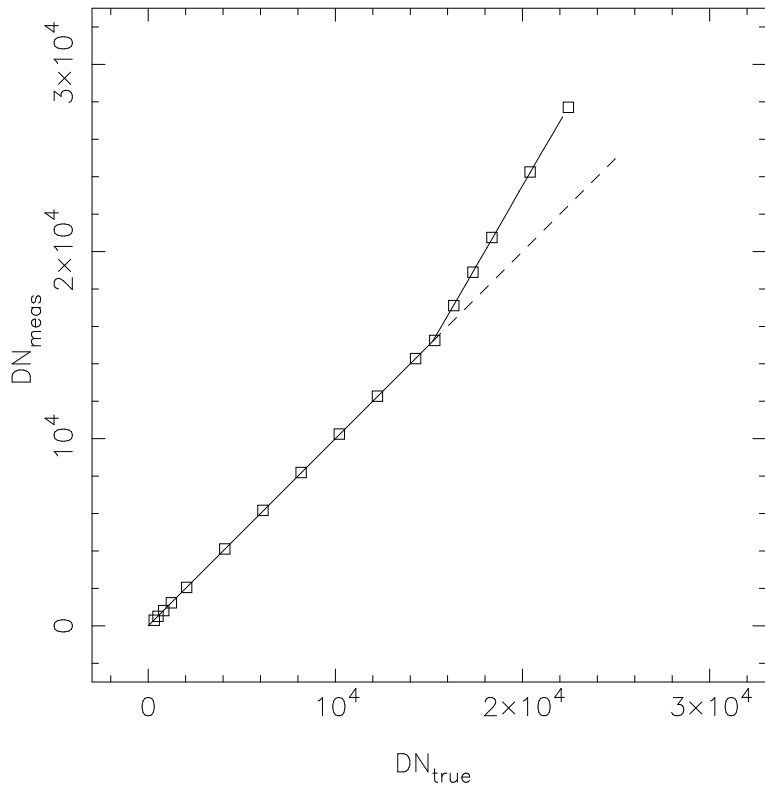


Fig. 1.— The linearity curve for the TK1024 CCD used on the USNO 1.0-m telescope for this program (solid line). DN_{meas} is the raw, bias-subtracted value of the signal; DN_{true} is the value that would have been measured if the CCD were completely linear. Note the “knee” at $DN \approx 15,200$ ADU. The dashed line acts as a reference for what a fully linear relation would look like.

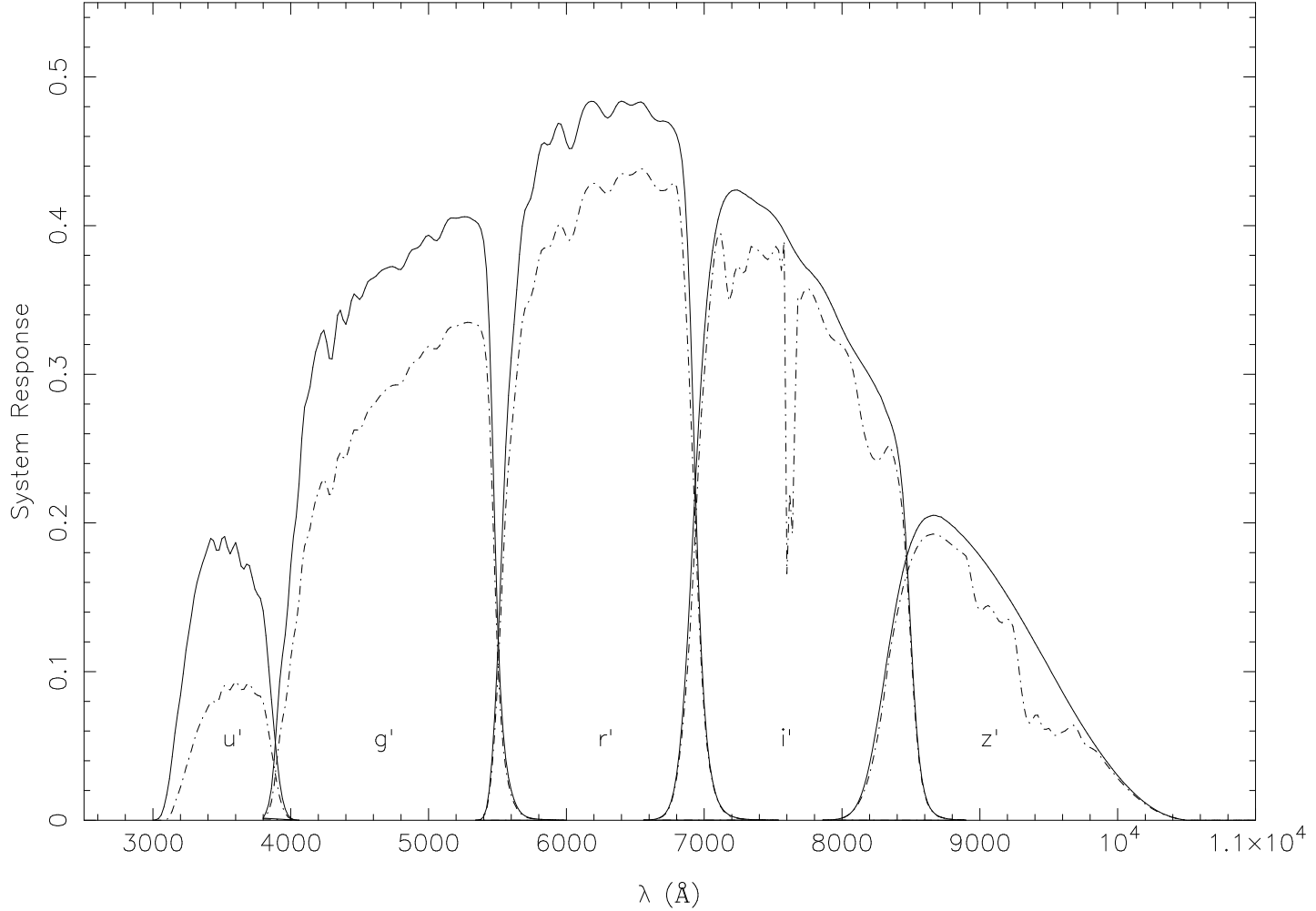


Fig. 2.— The $u'g'r'i'z'$ system filter bandpasses convolved with a typical coated CCD. The curves represent the expected total quantum efficiencies of the camera plus telescope on the sky. Solid curves indicate the response function without atmospheric extinction; dashed curves include extinction at 1.2 airmasses at the altitude of the U.S. Naval Observatory's Flagstaff Station.

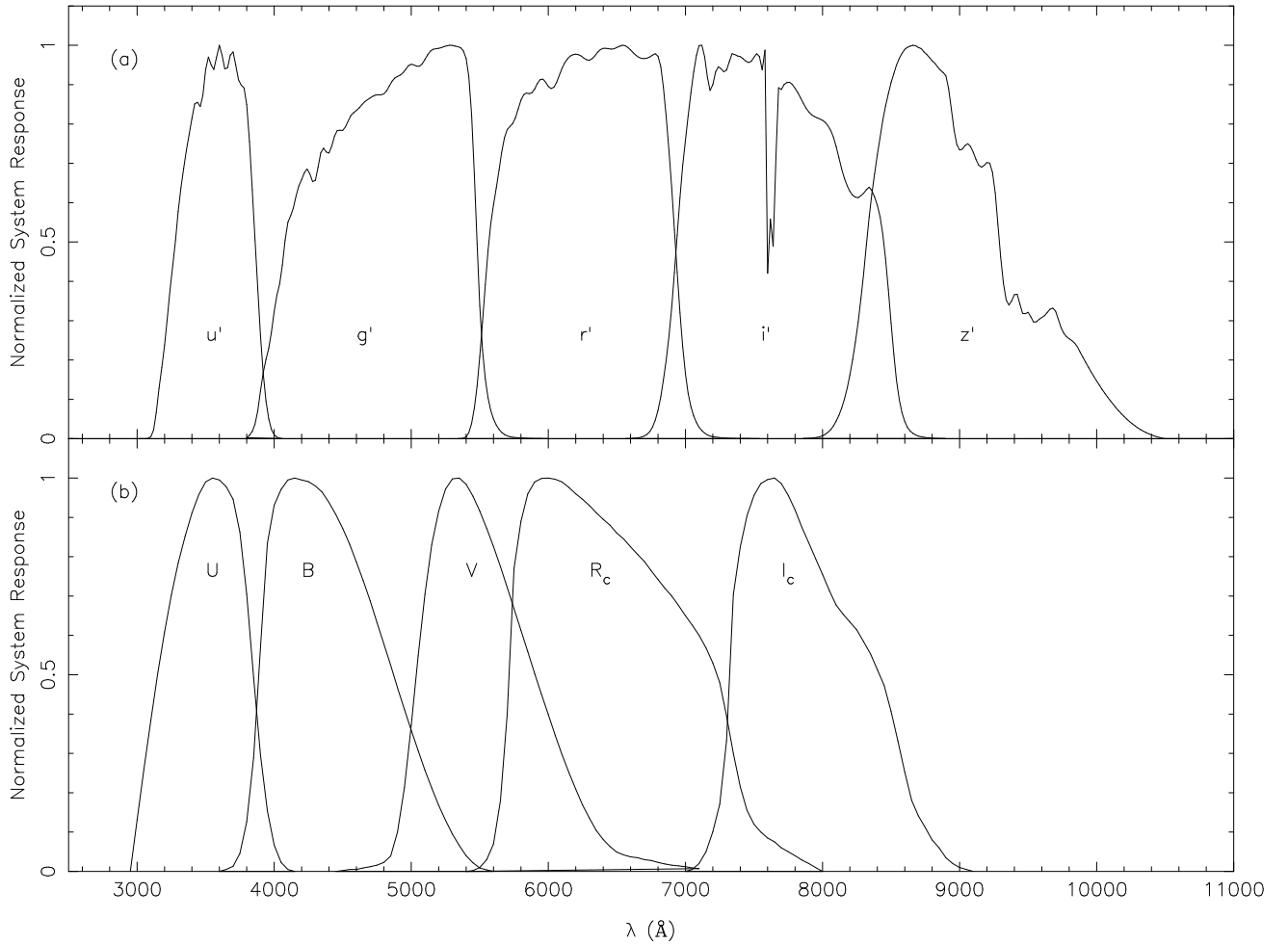


Fig. 3.— The (normalized) responses of the $u'g'r'i'z'$ system bandpasses (at 1.2 airmasses of extinction) compared those of the the Johnson-Morgan-Cousins ($UBVR_cI_c$) system. (Filter curves for the Johnson-Morgan UBV filters and for the Cousins R_cI_c filters were obtained from The General Catalogue of Photometric Data at <http://obswww.unige.ch/gcpd/gcpd.html>; Mermilliod, Mermilliod, & Hauck (1997).)

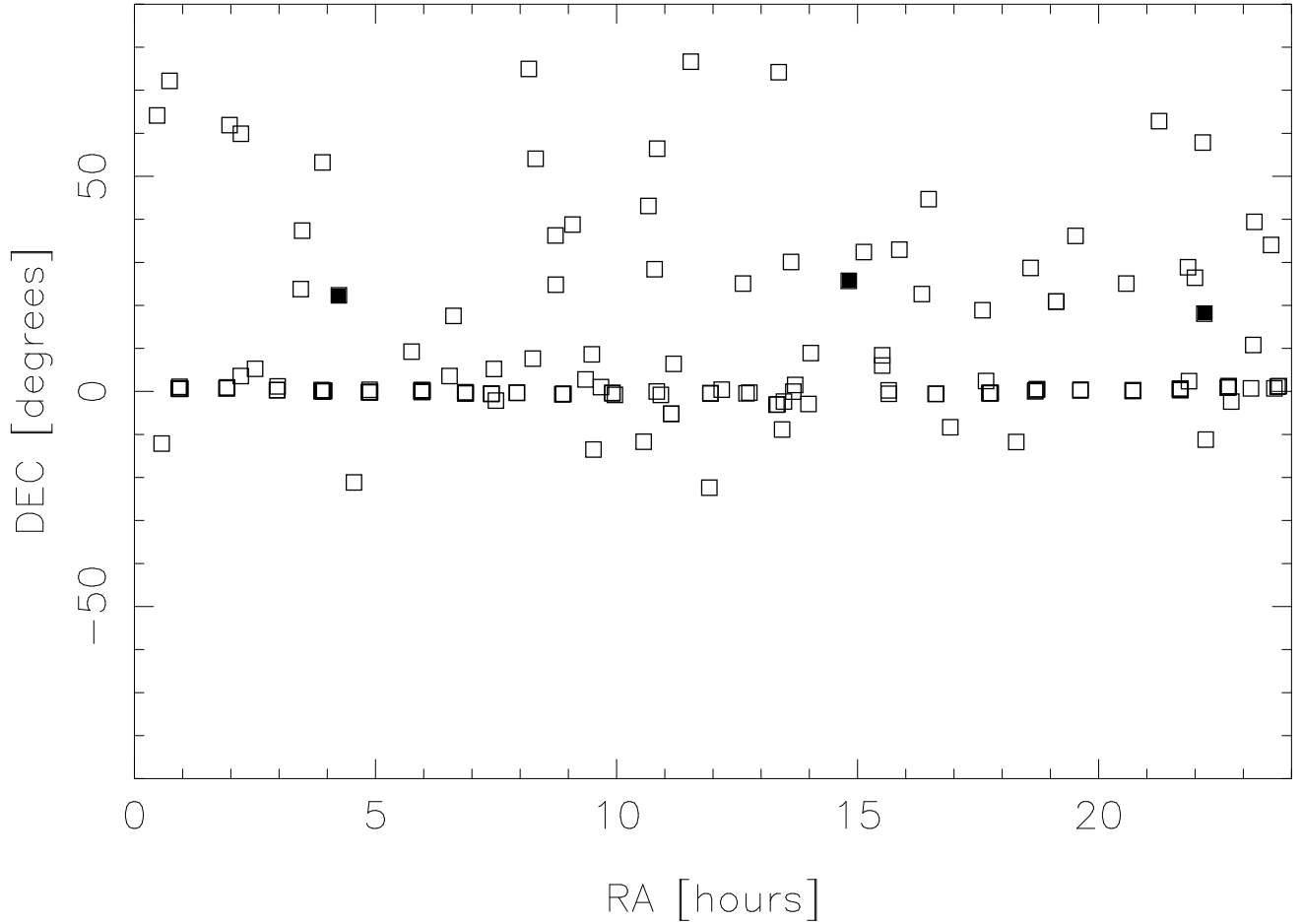


Fig. 4.— The distribution of the primary standards in right ascension and declination. Clearly seen are the clustering of stars near the celestial equator and the relative dearth of standards in the southern hemisphere. Most of the equatorial fields contain multiple stars therefore, though there are 158 stars in the system, there are not as many individual points on this plot. The three fundamental standards — BD+17°4708, BD+26°2606, and BD+21°0607 are indicated by the filled symbols.

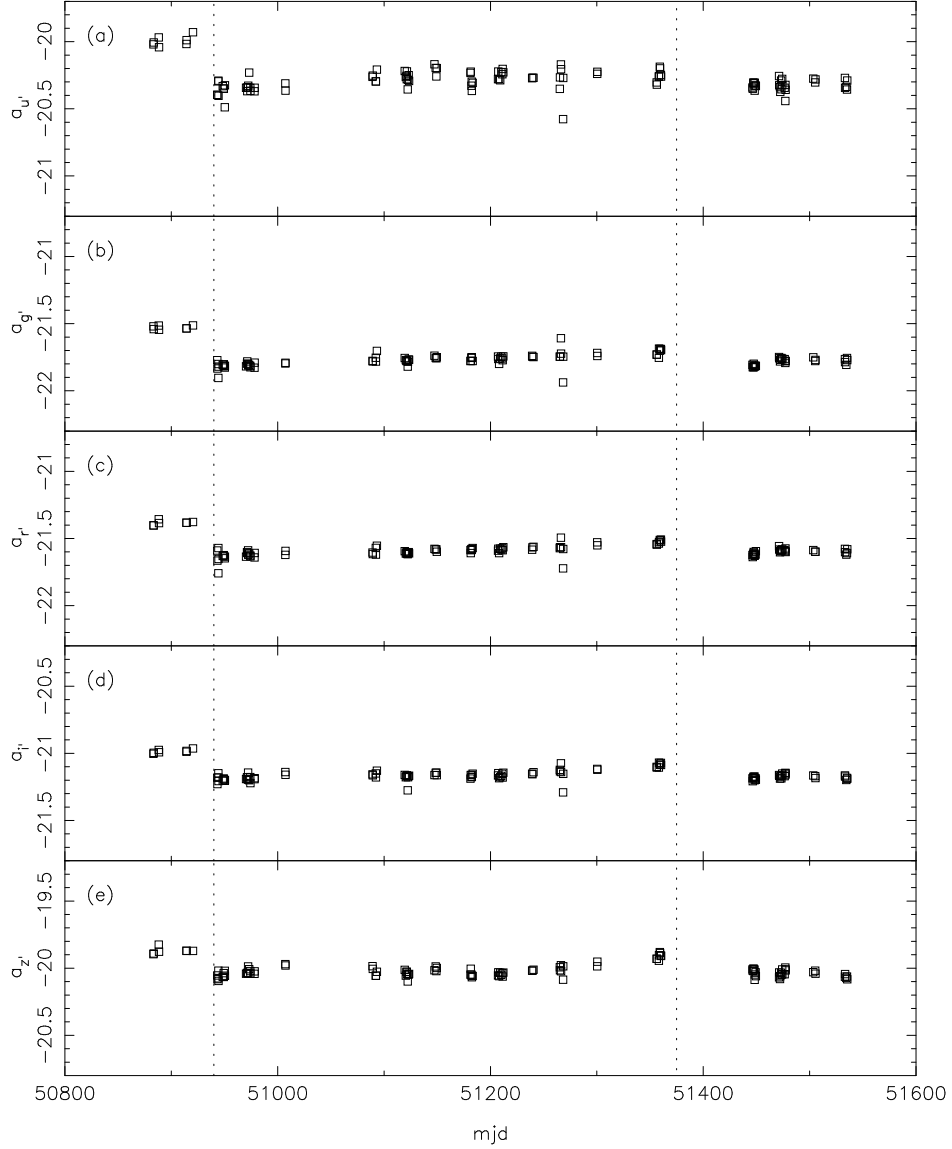


Fig. 5.— The photometric zeropoints calculated for each night of data used in developing the standard star network. The mirrors were re-aluminized twice during our program — once after the second month of observations and again prior to the last four months of observations (denoted by the dotted vertical lines). The first re-aluminization is clearly visible as a break in the zero point values while the second break is less obvious. The two large gaps (\approx mjd5100–51100 and mjd51350–51450) correspond to the two monsoon seasons (summers) in northern Arizona.

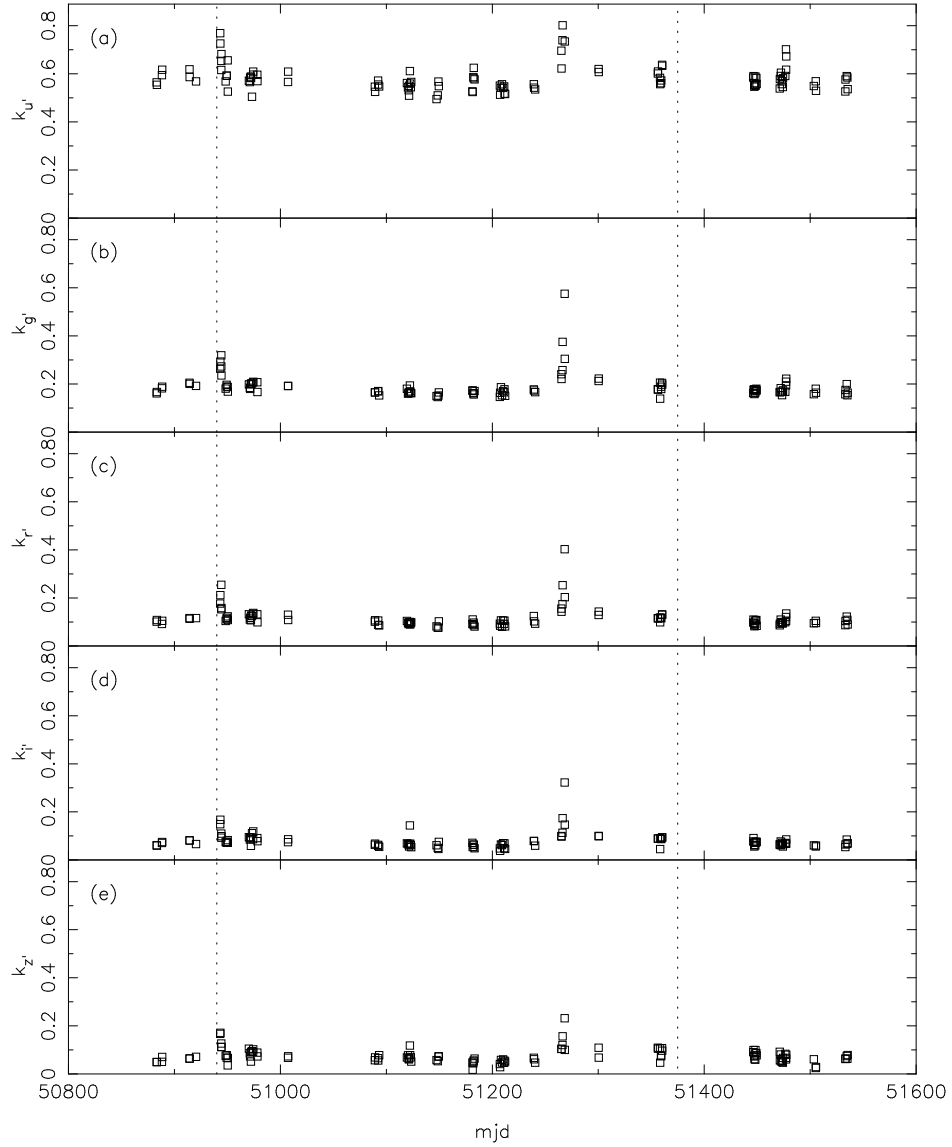


Fig. 6.— The primary extinction coefficients for each block of data used in developing the standard star network. The five nights with high extinction values (mjd50943, 51265, 51266, 51268 and, 51477) correspond to the night with low zeropoints. The times when the mirror was re-aluminized are denoted by the two dotted vertical lines.

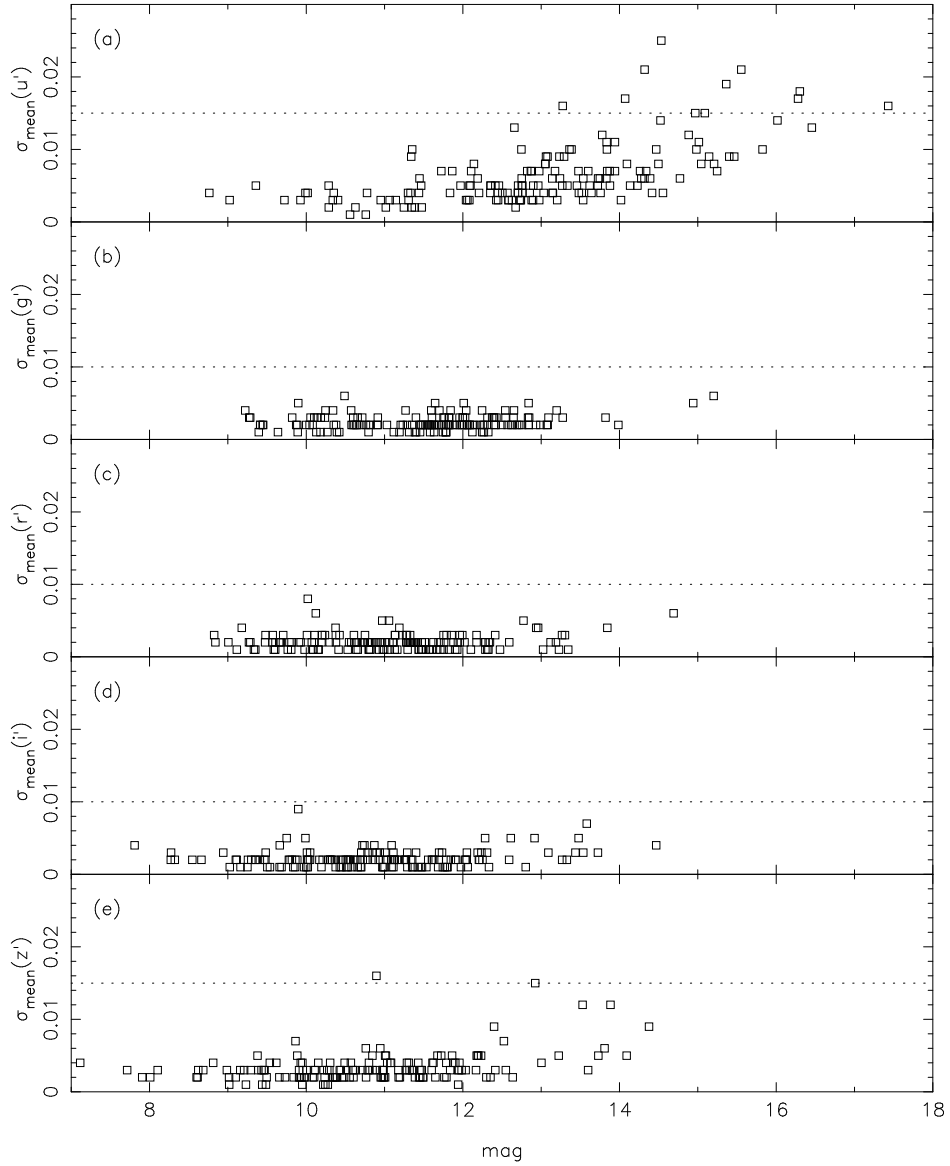


Fig. 7.— Mean error vs. magnitude ($\sigma_{\text{mean}}(u')$ vs. u' , $\sigma_{\text{mean}}(g')$ vs. g' , $\sigma_{\text{mean}}(r')$ vs. r' , $\sigma_{\text{mean}}(i')$ vs. i' , $\sigma_{\text{mean}}(z')$ vs. z'). The horizontal dashed lines are the survey requirement for the standard network to meet.

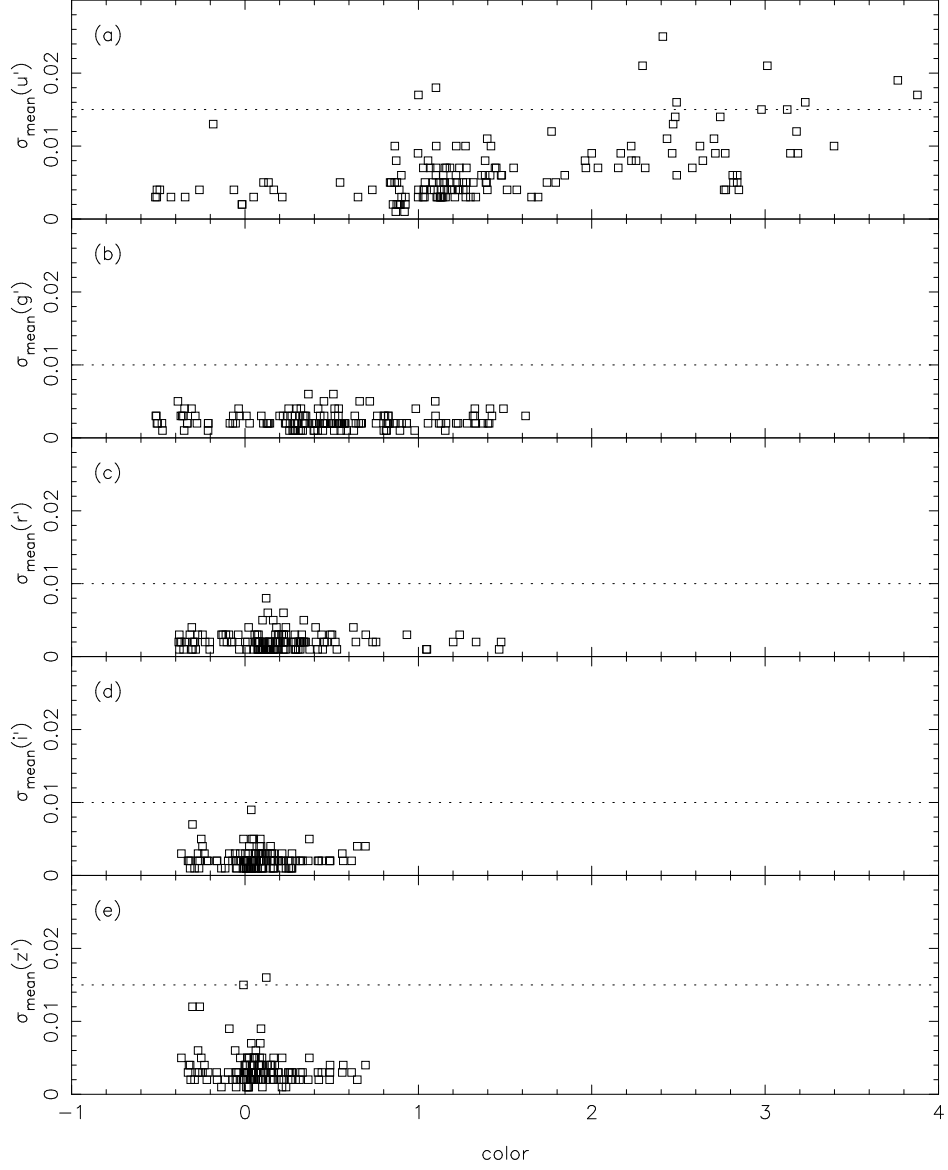


Fig. 8.— Mean error vs. color plot ($\sigma_{\text{mean}}(u')$ vs. $(u' - g')$, $\sigma_{\text{mean}}(g')$ vs. $(g' - r')$, $\sigma_{\text{mean}}(r')$ vs. $(r' - i')$, $\sigma_{\text{mean}}(i')$ vs. $(i' - z')$, $\sigma_{\text{mean}}(z')$ vs. $(i' - z')$). The horizontal dashed lines are the survey requirement for the standard network to meet.

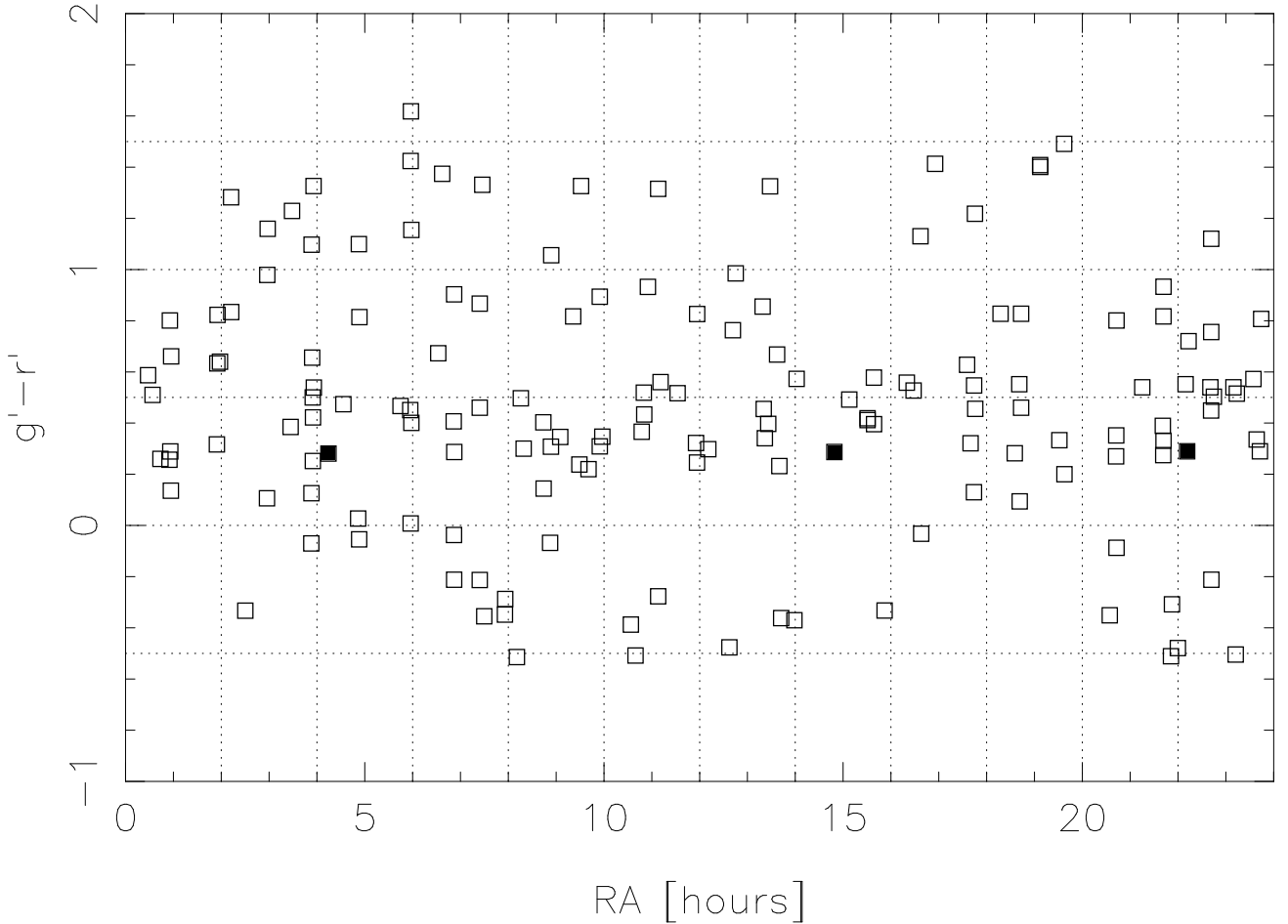


Fig. 9.— The distribution in $g' - r'$ vs. right ascension space for the 158 $u'g'r'i'z'$ primary and fundamental standards (the three filled symbols mark the positions of the three fundamental standards). Gridlines demark boxes 0.5 mag wide in $g' - r'$ and 2 hours wide in right ascension. Note that almost each box in the range $-0.5 < g' - r' < 1.5$ contains one or more standard stars.

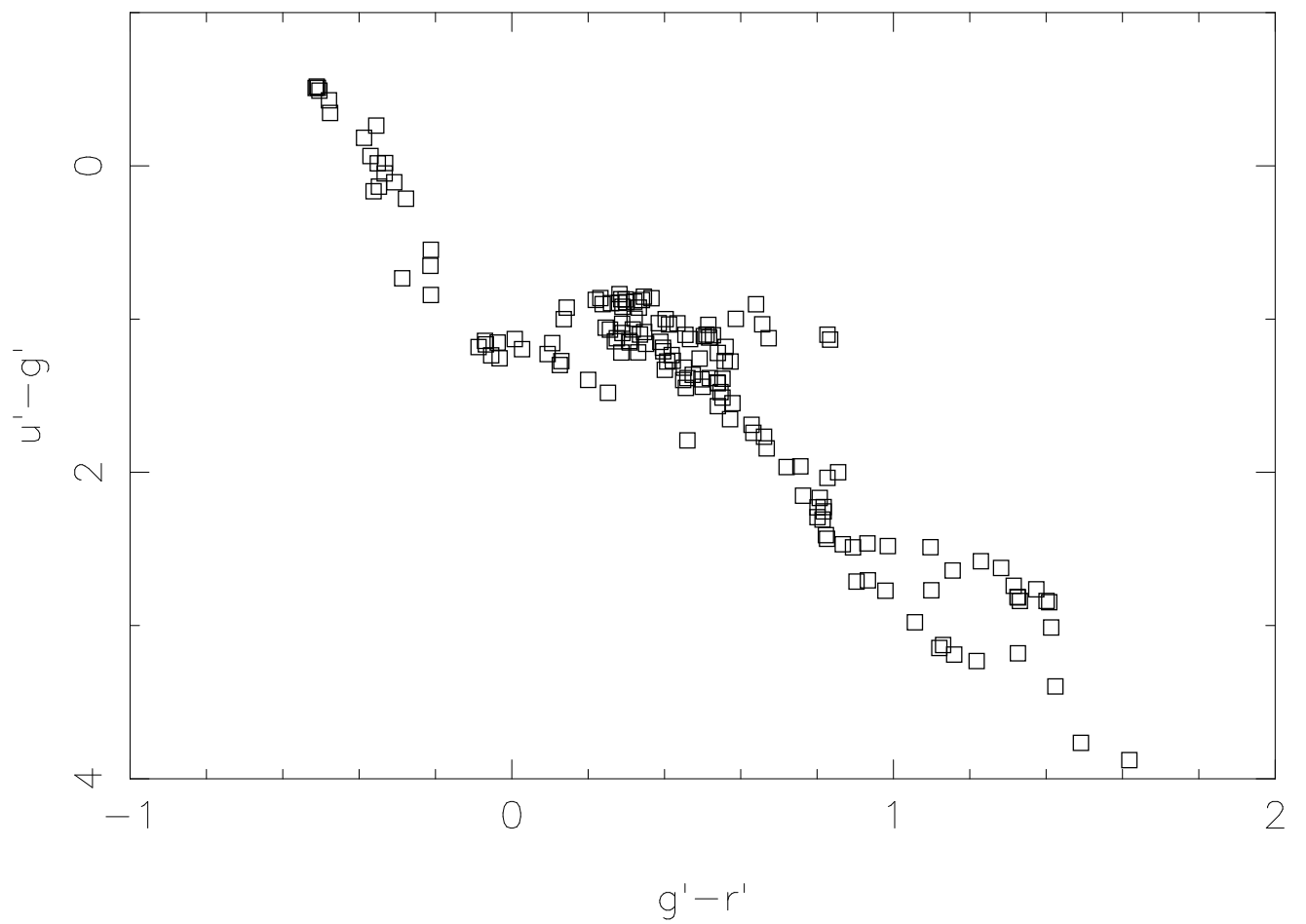


Fig. 10.— The $(u' - g')$ vs. $(g' - r')$ color-color plot for the 158 $u'g'r'i'z'$ standard stars.

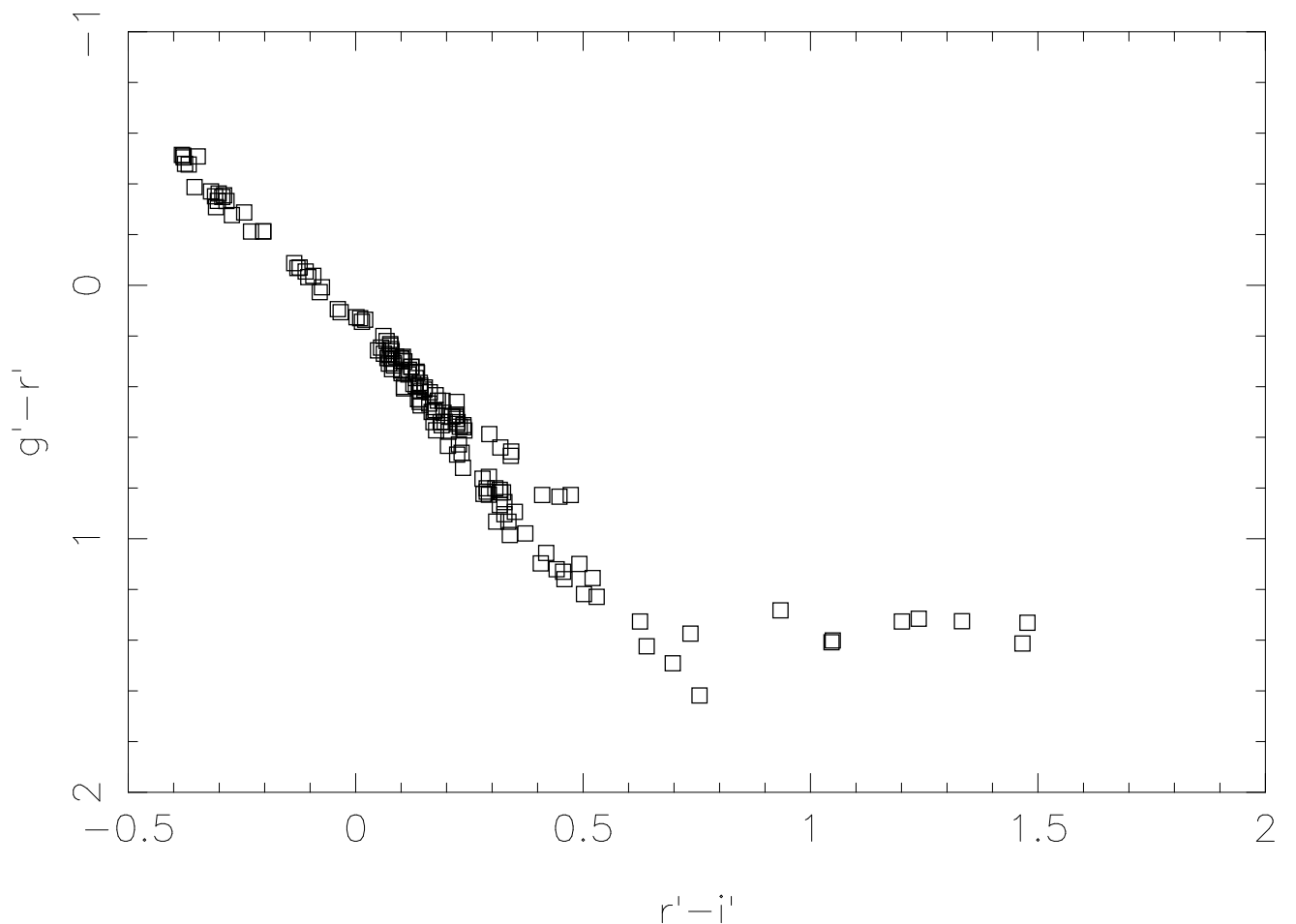


Fig. 11.— The $(g' - r')$ vs. $(r' - i')$ color-color plot for the 158 $u'g'r'i'z'$ standard stars.

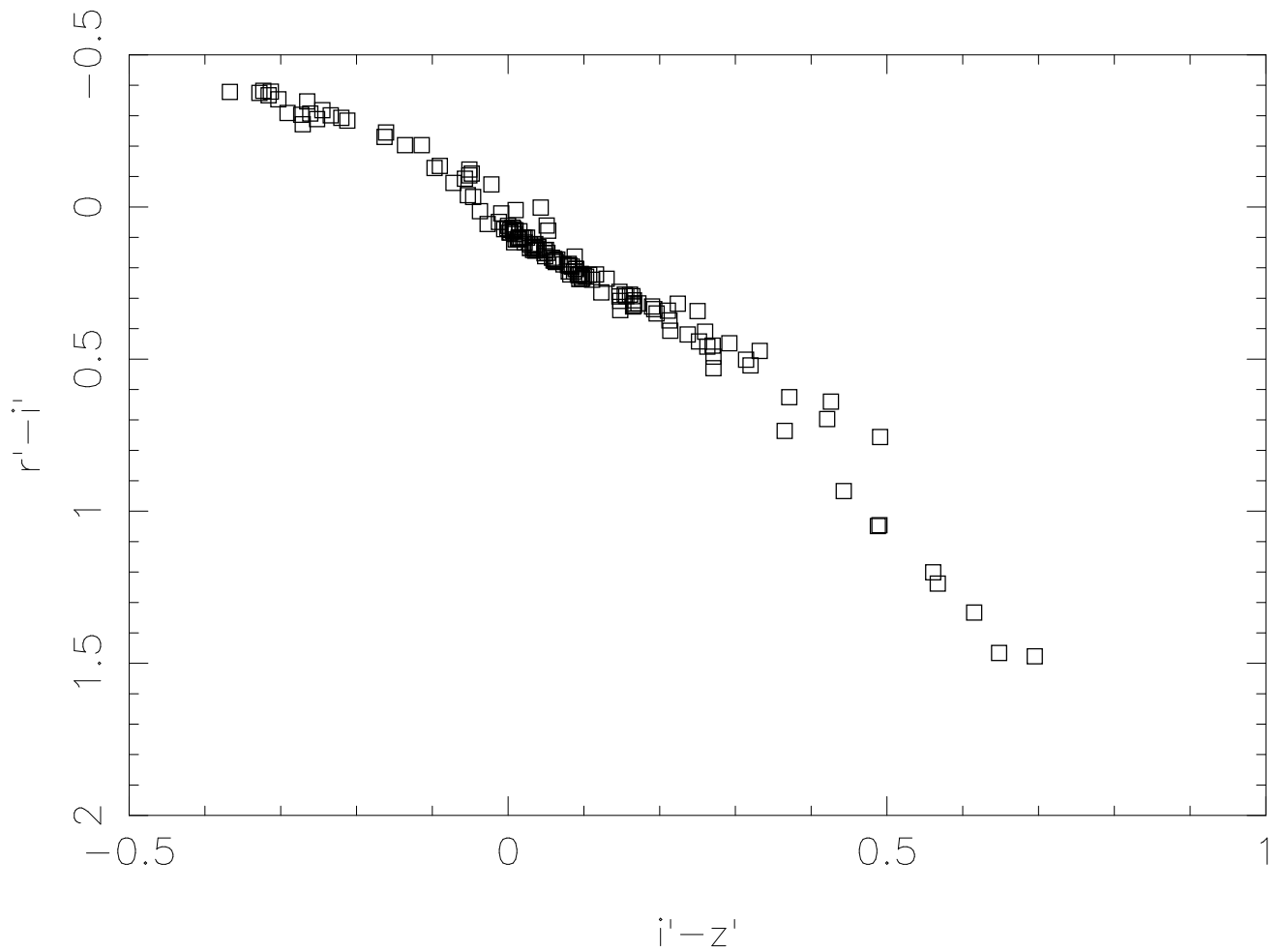


Fig. 12.— The $(r' - i')$ vs. $(i' - z')$ color-color plot for the 158 $u'g'r'i'z'$ standard stars.

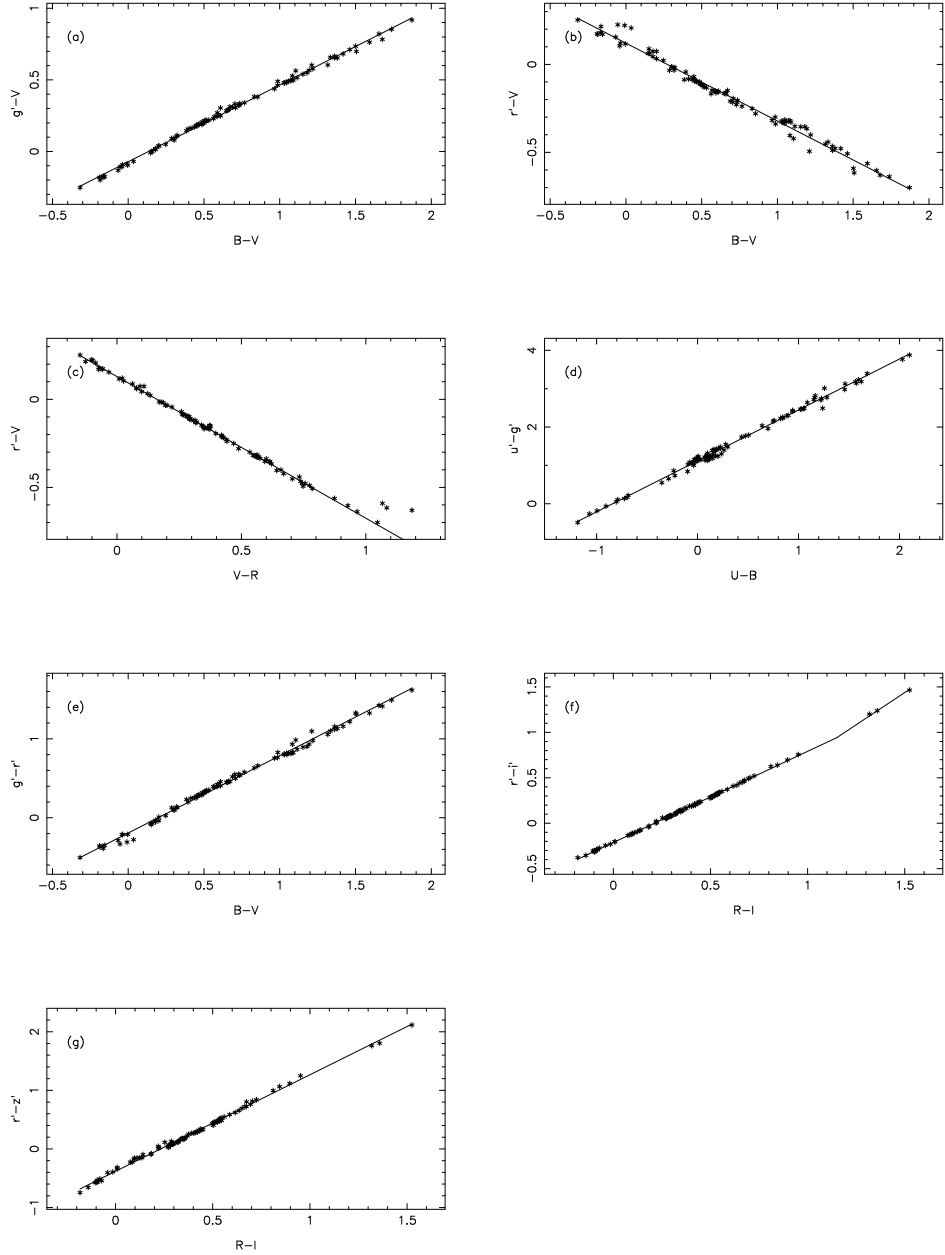


Fig. 13.— Comparison of $u'g'r'i'z'$ and $UBVR_cI_c$ magnitudes for those $u'g'r'i'z'$ standards measured by Landolt. The solid lines denote the linear fits listed under the “Observed” column of Table 7 for the $UBVR_cI_c \rightarrow u'g'r'i'z'$ transformations.

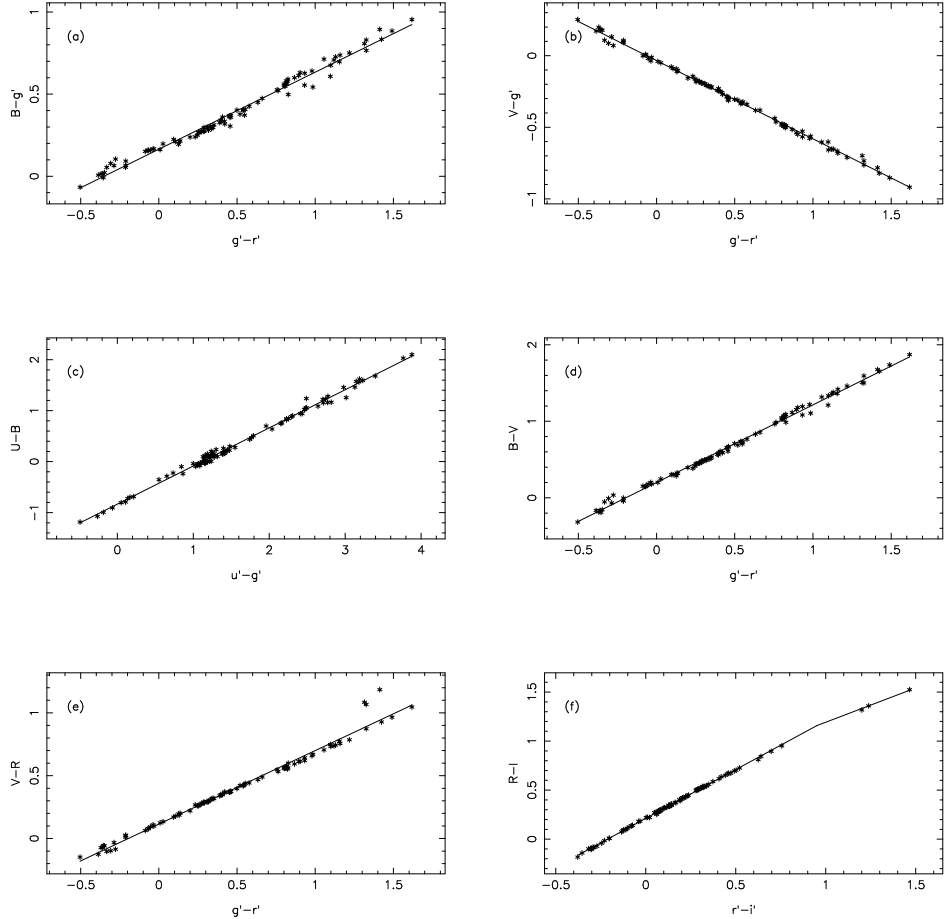


Fig. 14.— Comparison of $u'g'r'i'z'$ and $UBVR_cI_c$ magnitudes for those $u'g'r'i'z'$ standards measured by Landolt. The solid lines denote the linear fits listed under the “Observed” column of Table 7 for the $u'g'r'i'z' \rightarrow UBVR_cI_c$ transformations.

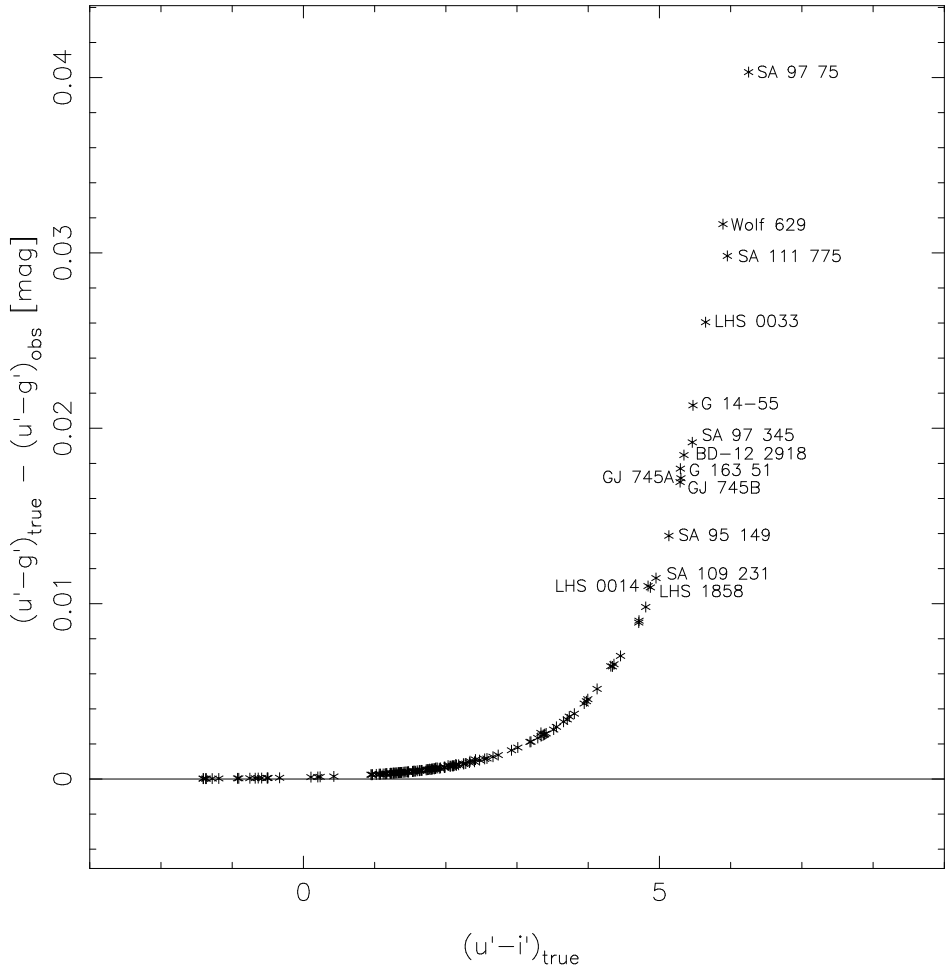


Fig. 15.— The red leak correction $[(u' - g')_{\text{true}} - (u' - g')_{\text{obs}}]$ vs. the red-leak-corrected $(u' - i')$ colors for all 158 $u'g'r'i'z'$ standards. Note that, for all but a handful of stars, the red leak correction is less 0.01 mag. Those stars with a red leak correction greater than 0.01 mag are explicitly labelled.